J. Fluid Mech. (2002), *vol.* 471, *pp.* 1–32.
DOI: 10.1017/S0022112002001647 Printed in the United Kingdom

An experimental study on hurricane mesovortices

By MICHAEL T. MONTGOMERY[1], VLADIMIR A. VLADIMIROV[2] AND PETR. V. DENISSENKO[2]

[1]Department of Atmospheric Science, Colorado State University, Fort Collins, CO 80523, USA

[2]Department of Mathematics, The University of Hull, Cottingham Road, Hull, HU6 7RX, UK

(Received 30 April 2001 and in revised form 8 May 2002)

Mesovortices in the eyewall region of a hurricane are intriguing elements of the hurricane engine. *In-situ* measurements of them are sparse, however, and our understanding of their overall role in the physics of a hurricane is incomplete. To further understand their dynamics an experimental apparatus using a homogeneous fluid (water) has been constructed to emulate the lower tropospheric flow of the hurricane eye/eyewall region.

For experimental configurations possessing a central aspect ratio less than unity, a primary and secondary circulation similar to the inflow layer of an intense hurricane, and a similar radius-to-width ratio of the curvilinear shear layer bordering the eye and eyewall region, the flow supports two primary quasi-steady vortices and secondary intermittent vortices. The vortices form through Kelvin–Helmholtz instability of the curvilinear shear layer bordering the slowly upwelling fluid in the centre and the converging fluid from the periphery. The primary vortices are maintained by convergence of circulation from the periphery and merger of secondary vortices spawned along the shear layer.

The horizontal flow field is measured using a particle image velocimeter. Despite the relatively strong secondary circulation through the parent vortex the horizontal flow is found to be approximately uniform in the direction parallel to the rotation axis. The peak tangential velocity is found to occur in the mesovortices and is roughly 50% greater than the parent vortex that supports them. The measurements provide insight into recent observations of excessive wind damage in landfalling storms and support the hypothesis that intense storms contain coherent vortex structures in the eyewall region with higher horizontal wind speeds locally than the parent hurricane.

1. Introduction

Hurricanes are a menace to life and property in populated coastal areas. The threat of storm surge and high winds is known for intense storms, but recent observations and numerical modelling studies are furnishing new insight into their structure by revealing multi-scale wind features ranging from sub-kilometre horizontal-scale wind streaks in the boundary layer (Wurman & Winslow 1998), 10 km horizontal-scale spiral wave features extending through the depth of the troposphere (Gall, Tuttle & Hildebrand 1998; Chen & Yau 2001; Wang 2002*a*, *b*), and 'eyewall mesovortices' near the storm's eyewall extending from the boundary layer to possibly the mid-troposphere (Marks & Black 1990; Black & Marks 1991; Willoughby & Black 1996;

Stewart & Lyons 1996; Stewart, Simpson & Wolff 1997; Hasler *et al.* 1997; Braun 2002; Kossin, McNoldy & Schubert 2002). Although wind streaks, spirals and mesovortices may appear unrelated, we believe they are connected to the vorticity dynamics of the hurricane eyewall region. To become better informed about the potential hazards of eyewall mesovortices and as a first step towards understanding their overall role in the physics of a hurricane we focus here on their fluid dynamics.

Eyewall mesovortices possess horizontal scales smaller than the diameter of the eye yet are of similar size or larger than the individual cumulus clouds that constitute the eyewall. While intriguing scientifically, they are also of significant practical concern. Originating in the quasi-circular shear layer just inside the eyewall and believed to form via Kelvin–Helmholtz (barotropic) instability of this curvilinear shear layer, eyewall mesovortices pose a threat to the safe operation of reconnaissance aircraft (Marks & Black 1990; Black & Marks 1991). Mesovortices concentrate the angular momentum of the parent vortex into a relatively small area and can produce swaths of heightened destruction for intense landfalling hurricanes when juxtaposed with convective downdraughts or boundary layer rolls (Wakimoto & Black 1994; Willoughby & Black 1996). Eyewall mesovortices are analogous to the 'suction vortices' of tornadoes (Fujita 1971; Rotunno 1984; Finley 1997; Fiedler 1998).

Eyewall mesovortices are believed to contribute to the thermal structure of the hurricane eye region. Since a hurricane vortex is in approximate gradient and hydrostatic balance (Willoughby 1990), its decrease of tangential wind with height requires that the eye temperature be greater than that of the eyewall. For the eye to be warmer than the eyewall at the same height level, subsidence forced by the inward flux of eddy angular momentum is believed to be necessary (Emanuel 1997, Appendix). Mesovortices, and the instability processes that spawn them, are thought to be the primary agents that accomplish this angular momentum flux (Schubert *et al.* 1999; Chen & Yau 2001; Kossin & Schubert 2001; Wang 2002*a*, *b*).

It is currently unknown whether mesovortices and related eddy processes generally limit or augment the intensification rate and maximum intensity of a hurricane. On the one hand, eyewall mesovortices may limit the intensity of a hurricane relative to the theoretical maximum intensity it would attain in their absence. The basis for this hypothesis can be illustrated by recalling the nearly inviscid solution for the zonally symmetric Hadley cell (overturning circulation and associated subtropical zonal jet in the Earth's tropical troposphere). In the Hadley cell problem, eddies caused by dynamic instability of the zonal mean flow are argued to be essential for reducing the strength of the subtropical jet to realistic (observed) values (Schneider 1977; Held & Hou 1980; Lindzen 1992, Chap. 7). Because of the similarity between the Hadley cell and hurricane problems one might anticipate a similar outcome in the hurricane problem. Recent numerical simulations support the notion of an 'eddy governor' (Schubert *et al.* 1999; Shapiro 2000). Barring adverse oceanic or environmental effects, these findings suggest that eddy processes near the eyewall of a mature storm may act to limit the intensity of the hurricane to realistic (observed) values. Eyewall mesovortices and related eddy processes may thus produce a negative feedback on the mean tangential velocity at the radius of maximum tangential wind (RMW).

On the other hand, eyewall mesovortices may be essential for a hurricane's rapid intensification and attainment of maximum intensity. This hypothesis is based on the outcome of certain sensitivity experiments using simplified axisymmetric numerical hurricane models employing a parameterization of moist-convective and eddy processes. The main parameters currently believed to control the maximum intensity of a hurricane are the sea surface temperature, tropopause temperature and relative

humidity of the subcloud layer (Emanuel 1986, 1995). ('Maximum intensity' is defined here as the maximum tangential velocity of the azimuthal and temporal mean vortex.) In these models quasi-horizontal fluid dynamical processes associated with vortex waves, Kelvin–Helmholtz instability, mesovortices and vorticity mixing is strictly non-existent; however, 'turbulence' of this kind is parameterized (using diffusive closure or numerical filtering) as a means of representing the radial transport of absolute angular momentum into the eye by these 'eddy' motions.

When these axisymmetric numerical models are run with a small but non-zero radial diffusivity of angular momentum, an initial vortex of finite amplitude intensifies to a hurricane whose intensity is consistent with thermodynamical parameters (Ooyama 1969; Emanuel 1989, 1997). With zero diffusivity, however, the initial vortex develops more slowly and attains an intensity well below the theoretical maximum predicted by axisymmetric theory (Emanuel 1989, § 3b; Emanuel 1997; and independent numerical experiments using a re-coded version of Ooyama's 1969 model, J. Camp, private communication). The explanation for the reduced intensity is that without parameterized eddy angular-momentum transport into the eye, a circular vortex sheet develops just inside the RMW preventing further contraction of the RMW by the low-level inflow. If the 'inertial wall' can be broken down, however, the tangential winds in the eye will intensify by inward eddy transport which in turn leads to an increase in the ocean-to-atmosphere entropy flux there. An enhanced entropy flux near and inside the RMW increases the mean subcloud layer entropy, that in turn increases the negative radial gradient of mean subcloud layer entropy, which is proportional to the square of the mean tangential wind at the RMW (Emanuel 1997). According to this model, then, 'momentum diffusion' into the eye has a positive feedback on the mean tangential velocity at the RMW.

Direct numerical simulations and non-neutral plasma experiments have furnished useful insight into the two-dimensional fluid dynamics of unforced unstable curvilinear shear layers (Huang, Fine & Driscoll 1995; Schubert *et al.* 1999; and references therein). For a circular shear layer (vortex ring) whose ratio of inner-to-outer radius is consistent with the observed tangential velocity distribution of a mature hurricane, the life cycle begins with the roll-up of the vorticity ring into several mesovortices by Kelvin–Helmholtz instability of the curvilinear shear layer (Michalke & Timme 1967). After several vortex turnaround times, the mesovortices become strained by the radial shear of the swirling flow and begin merging via chaotic advection. At long times ($t \geqslant$ several turnaround times of the mean vortex) the vortex re-consolidates into an approximate monopole and weakens in terms of maximum tangential velocity. The end state of this vorticity redistribution process can be predicted using global selective decay ideas.

Further research using a hierarchy of models is under way to understand the modification of this process by details of the initial condition (e.g. narrow versus broad vortex rings (Schecter *et al.* 1999; Kossin & Schubert 2001)), secondary vorticity rings outside the primary eyewall (Kossin, Schubert & Montgomery 2000), and three-dimensional effects (Nolan & Montgomery 2002). These studies help clarify the vorticity dynamics that are believed to operate in a hurricane vortex whose mean secondary circulation that maintains the vortex against frictional dissipation has become suppressed in association with increased environmental vertical shear, landfall, reduced sea surface temperature, or the formation of a secondary (outer) eyewall.

With a sustained secondary circulation, such as in an intensifying or quasi-steady hurricane, the fluid dynamics is considerably richer than its unforced counterpart. In

this case the mesovortices tend to be sustained by the convergence of circulation from the periphery, vortex-tube stretching, and downwelling near the axis of symmetry. New questions arise about the mesovortices in the 'forced flow' regime:

(i) What is the instability mechanism that produces them?
(ii) What is their structure?
(iii) Are they stable coherent structures?
(iv) How do their local wind speeds compare with that of the parent vortex?
(v) How many are to be expected?

To help answer these questions we have constructed an 'upside down' hurricane simulator. The apparatus (see figures 3 and 4) is designed to furnish an azimuthal mean tangential and radial velocity distribution that is consistent with the known lower-tropospheric mean inflow and interior shear-layer structure of an intense hurricane. The two-celled vortex flow is shown to support two quasi-permanent mesovortices whose circulation constitutes a significant fraction of the core's total circulation. The mesovortices are maintained by convergence of circulation from the environment and downwelling in the central region. The structure and intensity of the mesovortices is measured with a particle image velocimeter (PIV). The central part of the flow is visualized using standard methods. Our results support previous experimental and theoretical work by Vladimirov & Tarasov (1980, hereafter referred to as VT) and Gall (1983) suggesting that in low-aspect-ratio and high-swirl-ratio vortices with secondary circulation, such as hurricanes, the instability spawning the mesovortices and the ensuing dynamics are governed in the first approximation by quasi-two-dimensional fluid dynamics.

The plan of this paper is as follows. Section 2 presents observations that motivate the approach adopted here. Section 3 justifies the experimental strategy. Section 4 details the experimental apparatus. Section 5 presents flow visualizations. Section 6 summarizes the PIV setup. Section 7 presents the velocity measurements. Section 8 presents a two-dimensional stability analysis of the experimental flow. Section 9 presents the conclusions.

2. Observations of hurricane mesovortices

Recent observations suggest that hurricane mesovortices are ubiquitous. As an example figure 1 shows the eye of Hurricane Emilia (July, 1994) viewed from the Space Shuttle Columbia when Emilia was several hundred miles southeast of Hawaii. Emilia was an intense hurricane with sustained near-surface winds of $80\,\mathrm{m\,s^{-1}}$. An approximately circular eyewall cloud surrounds the eye. Two prominent mesovortices are evident in the lower troposphere with diameters nearly half the diameter of the eye.

A second example is furnished by Hurricane Alberto (2000), which was significantly weaker than Emilia. The eye region of Alberto viewed from the MODIS instrument aboard NASA's polar-orbiting TERRA satellite is shown in figure 2. At this time Alberto had an estimated near-surface wind speed of $43\,\mathrm{m\,s^{-1}}$ and was centred at 35.6 N lat., 48.4 W long. The eye is approximately 70 km in diameter. Noteworthy are the two prominent mesovortices in the lower troposphere located at the northern and southern edges of the eyewall cloud.

In addition to Space Shuttle photographs and satellite observations, aircraft penetrations into hurricanes provide important *in-situ* observational data. During aircraft penetrations into Hurricane Hugo (1989) at a flight altitude of 450 m, a NOAA WP-3D aircraft encountered an intense mesovortex near Hugo's eyewall. A report of this encounter is provided by Marks & Black (1990) and Black & Marks (1991) and a summary of the velocity data acquired during this encounter is given in Kossin

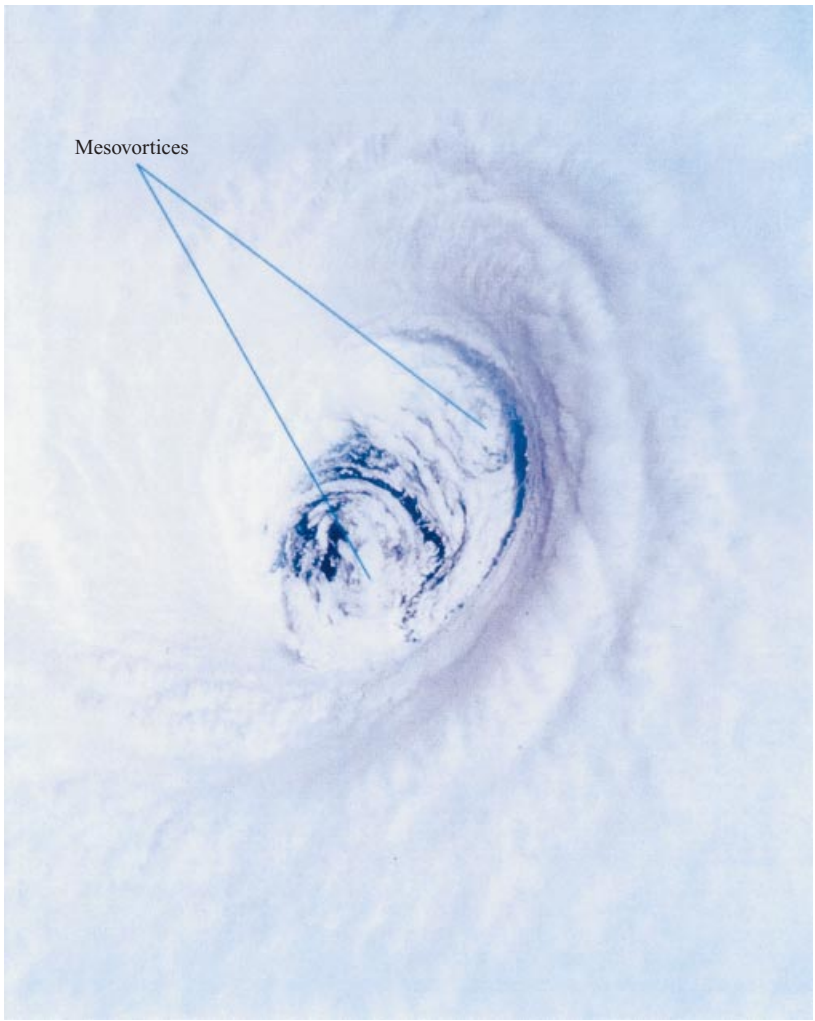

FIGURE 1. Hurricane Emilia's (1994) eye region as photographed aboard Space Shuttle Columbia when Emilia was several hundred miles southeast of Hawaii. It was an intense hurricane with eye diameter approximately 50 km and sustained near-surface winds of approximately 80 m s^{-1}. This photograph appeared on the cover page of *Weatherwise*, October/November 1996 issue. Photograph courtesy of NASA.

& Schubert (2001). The mesovortex is believed to have originated within a strong cyclonic shear region on the inside of the eyewall cloud where the radial shear of tangential velocity was approximately 60 m s^{-1} in less than 0.5 km.

The notion of important eddy exchange processes between the hurricane's eyewall and eye is not new (Malkus 1958; Kuo 1959; Gray & Shea 1973; Emanuel 1989, 1997). But the theoretical and observational evidence pointing to lateral mixing in association with quasi-two-dimensional mesovortices and vorticity mixing (Schubert *et al.* 1999; Kossin & Eastin 2001; Kossin & Schubert 2001; Kossin, McNoldy & Schubert 2002) is relatively new to this area.

3. Experimental strategy

Although direct numerical simulation is widely believed the most expedient means for obtaining quantitative information on hurricanes, and eyewall mesovortices in par-

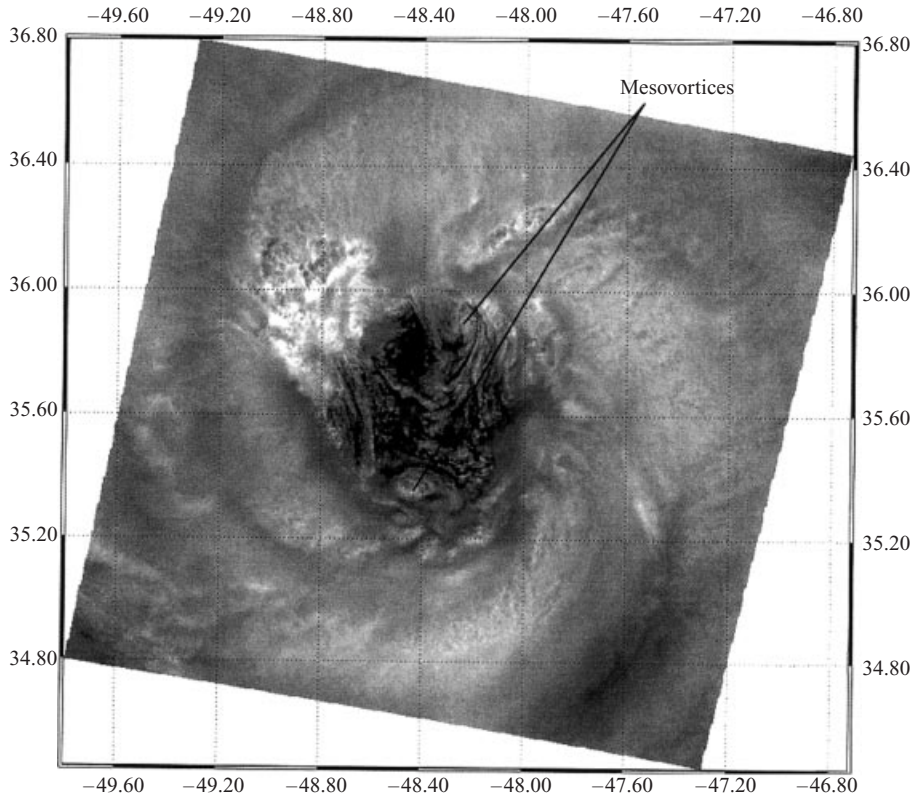

FIGURE 2. Hurricane Alberto's (2000) eye region as observed using Channel 2 of the Moderate Resolution Imaging Spectroradiometer (MODIS) aboard NASA's polar-orbiting TERRA satellite. The image was taken on August 20, 2000, 1415 UTC. Channel 2 (centred on 0.865 μm) was used because of its superior resolution of 250 m compared to 1 km for visible channels on current geosynchronous satellites. Photo courtesy of B. McNoldy and CSU/CIRA.

ticular, numerical models are not without uncertainties with respect to discretization errors, and the parameterization of turbulence, microphysical and sea–air transfer processes at high wind speeds (Emanuel 1995, 1998; Braun & Tao 2000; Hausman 2001). An experimental approach is believed useful because it provides an independent method of estimating the structure and intensity of the asymmetric flow of the hurricane eye/eyewall region under the idealized (control) condition of steady forcing.

Unlike a tornado which is driven externally by its parent thunderstorm, a hurricane is driven by energy sources internal to and on the boundary of the vortex (Riehl 1954; Ooyama 1969; Willoughby 1979; Shapiro & Willoughby 1982; Ooyama 1982; Emanuel 1986; Rotunno & Emanuel 1987). Modelling a complete hurricane requires representing the internal and boundary layer processes that establish the 'in-up-out' (secondary) circulation essential for maintaining the vortex against 'friction' at the ocean surface. The representation of cumulus convection and the attendant latent heat release in the hurricane's interior has been the primary obstacle preventing the successful laboratory modelling of a hurricane.

The current approach bypasses all questions associated with the moist processes that generate the primary and secondary flow. Rather than model a complete hurricane, we focus on its eye/eyewall flow in the lower troposphere. The large size disparity between a hurricane and any experimental apparatus generally prohibits strict dynamical

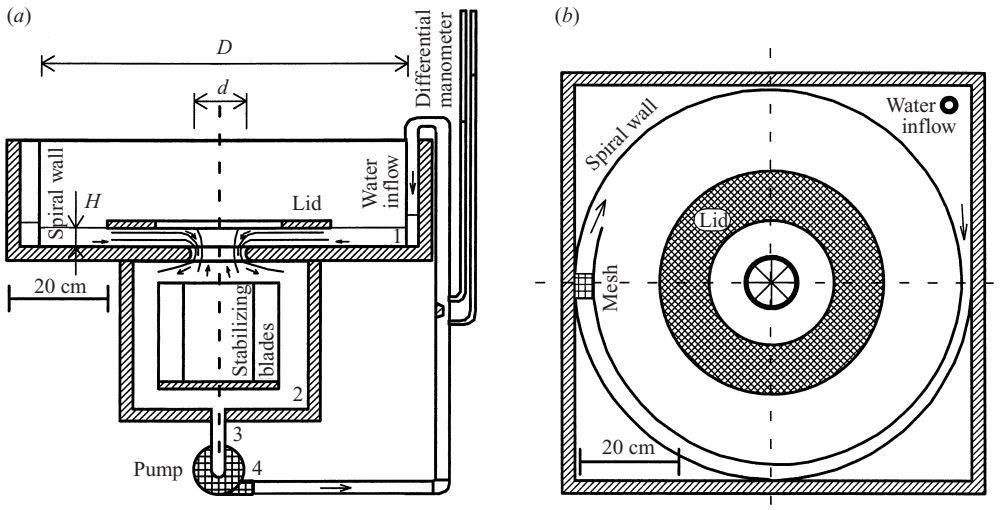

FIGURE 3. Schematic of experimental apparatus. (*a*) Sideview of setup. Lower boundary layer, upper boundary layer, upwelling flow, and return flow shown by arrows. (*b*) Plan view of setup. In upper vessel: source of water inflow, spiral channel, orifice at centre, upper lid (L). In lower vessel: cross blades. See § 4 for further details.

similitude. If the laboratory Reynolds number is sufficiently high, however, and the aspect ratio, mean inflow structure and radius-to-width ratio of the interior shear layer are kinematically similar then the experimental mesovortices should exhibit characteristics similar to real eyewall mesovortices.

4. The experimental apparatus

Previous experimental studies of intense (rapidly rotating) geophysical vortices have focused primarily on tornadoes, waterspouts and dust-devils (Ward 1972; Wan & Chang 1972; Church, Snow & Agee 1977; VT; Lugovtsov 1982). Geometrically speaking, these are long and thin vortices whose characteristic aspect ratio, defined by the ratio of the vortex height to core diameter, is typically large compared to unity (Morton 1966). Depending on experimental conditions, these vortices can spawn secondary or 'suction' vortices through the development of an instability of shear layers in the rotating flow (VT; Rotunno 1978; Michalke & Timme 1967; Weske & Rankin 1963). Experimentally simulated suction vortices resemble what is currently known about their atmospheric counterparts based on observations (Fujita 1971; Sinclair 1973) and numerical modelling studies (Rotunno 1984; Finley 1997; Fiedler 1998).

A hurricane, on the other hand, is a shallow and broad vortex whose characteristic aspect ratio is typically less than unity. A hurricane and the secondary vortices spawned within its core cannot be simulated easily with the original tornado chambers used by Ward (1972) and Church *et al.* (1977) without reconfiguring the experimental apparatus. A simpler and more direct model for simulating both types of vortices (i.e. long and thin or shallow and broad) has been presented previously by VT and a modified version of their apparatus has been constructed for this study.

Figures 3(*a*) and 3(*b*) present a side-view and plan-form schematic, respectively, of the experimental setup. A swirling flow of water contained in a cylindrical vessel (1) of diameter D and fluid depth H leaves through the opening at the centre of the bottom of this vessel and enters the lower vessel (2). The opening is a smooth circular

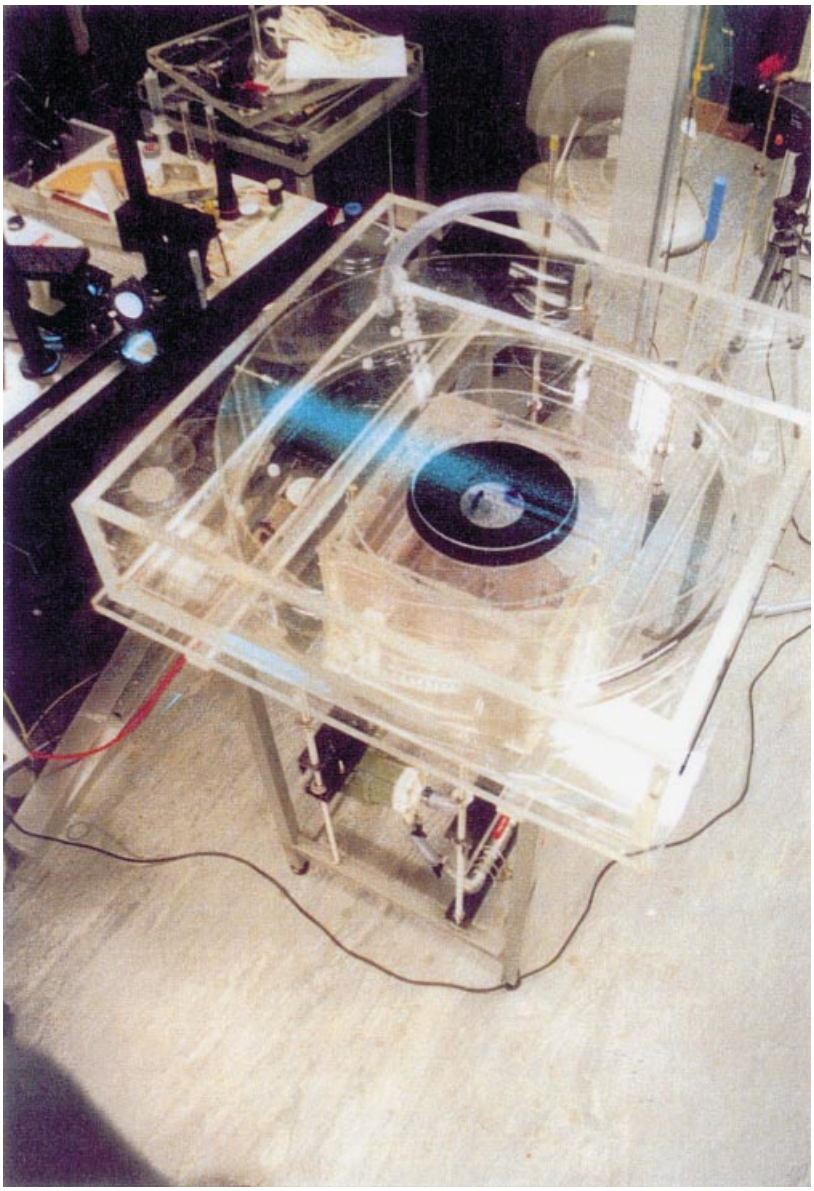

FIGURE 4. Photograph of experimental apparatus. Laser sheet mirror, water pump, and pair of primary mesovortices are evident in photograph.

orifice of diameter d. The smoothed orifice edges are 2.5 cm thick. A circular lid with a hole in its centre is placed at free-surface level. The lower vessel is a rectangular tank with a system of stabilizing blades from which the water is extracted by means of a hose (3). The stabilizing blades serve to suppress vortical motions generated from the upper vessel. The volume flow rate Q is a prescribed parameter via a pump that draws water from the lower vessel and returns it to the upper vessel through a spiral channel. The flow rate is measured by a manually calibrated differential manometer.

A photograph of the experimental apparatus is shown in figure 4. Constructed from Plexiglas, its dimensions are as follows. The upper chamber housing the cylindrical

vessel 1 is 80 cm by 80 cm with a height of 20 cm. The lower vessel 2 is 35 cm by 35 cm and is 30 cm in height. The perimeter bounding the fluid in the upper vessel is a circular wall of radius 40 cm for 180° of arc, changing to an Archimedes spiral for 360° of arc with a terminal radius of 36 cm (see figure 3*b*). While not crucial to the experiment, the Archimedes spiral initiates the mean radial velocity of the fluid as it leaves the curvilinear channel. Suspended by three vertical bolts, the upper lid has an outer diameter of 40 cm and an inner diameter of 25 cm. Since the viscous stress vanishes along the free surface, the region within the upper lid ($r < 12.5$ cm) emulates a 'semi-slip' (as opposed to a 'no-slip') boundary condition along the top of the surface layer in a hurricane (Eliassen & Lystad 1977; Shapiro 1983). Discrepancies between the experimental flow and real hurricanes outside the RMW are noted in § 7.

The orifice diameter d is chosen to be larger than the fluid depth H in vessel 1 in order to achieve geometrical similarity with the eye region of a real hurricane ($H < d$). Values employed for the benchmark experiment are $d = 10$ cm and $H = 4$ cm. All of the principal flow features described here are observed to be robust to changes in these parameters (e.g. doubling the depth for a fixed orifice diameter, increasing or decreasing the flow rate, or using a wider upper lid with same flow rate and aspect ratio) as long as the depth does not exceed the diameter of the orifice. When $H \geqslant d$ the core flow becomes strongly three-dimensional and the mesovortices coil into helical spirals starting from the bottom. The physics responsible for this flow bifurcation lies beyond the scope of the present study (see VT and Lugovtsov 1982 for example and discussion; an illustration of this phenomenon with a prototype of the current apparatus is also available; see footnote, p. 11).

The radius of penetration of the inflowing fluid is determined by the circular orifice at the bottom of vessel 1. For reasons described below, the orifice creates and maintains a curvilinear shear layer bordering the interior and exterior flow. The orifice produces an azimuthal mean transverse flow that is similar to an axisymmetric Ekman layer in a hurricane vortex that causes maximum boundary layer pumping just inside the RMW (Eliassen & Lystad 1977; Shapiro 1983). Vortex-tube stretching in the lower troposphere is greatest near this radius. If in either the experiment or a real hurricane the instability and eyewall mesovortices were artificially suppressed the mean vorticity distribution would collapse to a circular vortex sheet.

The influence of the orifice on the experimental flow has been described previously by VT and Lugovtsov (1982), but because of its importance in the present work we review the matter following VT. For the moment, let us assume the upper lid (L) in vessel 1 is not present. All flows of a rotating fluid above a solid surface at rest have a radial inflow along the bottom converging to the centre of rotation. The reason for such inflows is the existence of a radial pressure gradient associated with the swirling flow in the bulk fluid; recall, e.g., 'Bodewadt's swirling flow' consisting of a uniformly rotating fluid over a solid surface at rest (Schlichting 1960, pp. 176–180). In contrast to the spin-down problem in an ordinary vessel with continuous bottom boundary (Greenspan 1968), the flow from the bottom boundary layer in the current experiment does not return to the main flow, but passes through the opening into the lower vessel (see figure 3*a*). The behaviour of the fluid in the bottom boundary layer is due to the fact that it has greater angular momentum than the fluid in vessel 2, but less than that of the fluid in vessel 1.

In the central part of the opening one observes an ascending return flow (see figure 3*a*), the nature of which can be understood from the fact that the swirling fluid in the upper vessel has a lower dynamical pressure near the centre relative to that in the lower vessel, a so-called 'Archimedean' centrifugal force. The reduced pressure

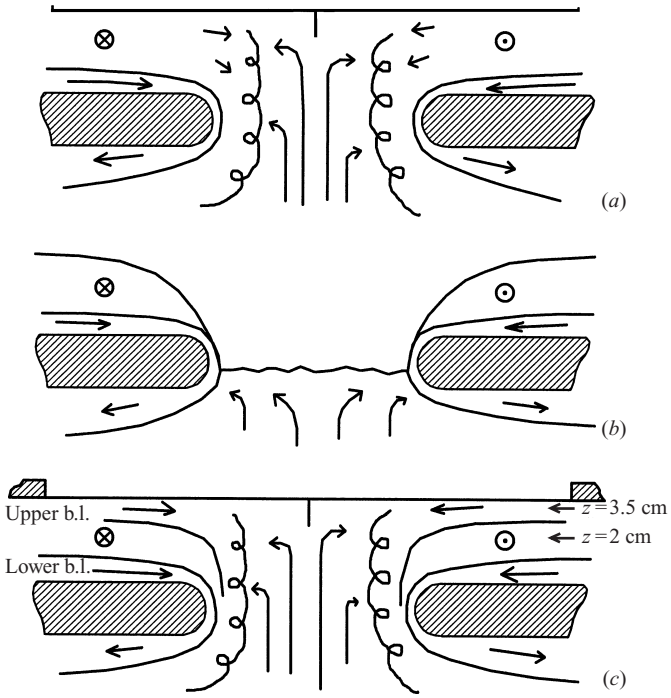

FIGURE 5. Schematic of three flow regimes observed with the experimental apparatus for core aspect ratio less than unity: (*a*) no lid, low flux; (*b*) no lid, high flux; (*c*) with lid, low flux. This study focuses on regime (*c*).

consequently sucks fluid from the lower vessel and gradually fills the cylindrical region around the symmetry axis in the upper vessel (figure 5*a*). When Q exceeds a sufficiently large value the flow in the upper vessel consists of a single vortex whose free surface curves down to the opening. The return flow is then confined to the lower vessel and can no longer collide with the fluid in vessel 1 (figure 5*b*). The value of Q employed for the benchmark experiment (with upper lid), however, is well below this critical value (figure 5*c*). (A prior study by Whitehead & Porter (1978) examined the problem of critical withdrawal of a rotating fluid, similar to figure 5(*b*), a supercritical flow regime near the centre. Whitehead & Porter's experimental apparatus (their figure 3) prevented the flow in the 'catch basin' from being sucked back into the main vessel above the orifice. This forbids the formation of the curvilinear shear layer and the attending mesovortices and related 'eddy' structures that are the focus of this paper.) The collision between the two flows, one from the lower vessel with zero angular momentum, and the other from the sidewalls with non-zero angular momentum, sets up an appreciable curvilinear shear layer in the horizontal velocity of the core flow. If the radial shear of the tangential flow is high enough, the flow is found to be unstable to small-amplitude asymmetric disturbances (VT; Lugovtsov 1982; Gall 1983; Rotunno 1984). Strictly speaking, however, with both a primary and secondary circulation one does not know *a priori* if the instability that produces the mesovortices is a two-dimensional Kelvin–Helmholtz instability as suggested by VT and Lugovtsov (1982) or a fully three-dimensional instability as argued by Rotunno (1984) for the case of tornadoes in certain parameter regimes. One of our objectives is to determine whether the instability mechanism responsible for the mesovortices is a two-dimensional or a three-dimensional mechanism. We take up this issue in § 8. The

instability results in multiple vortices that coexist with the mean tangential and radial flow. The nature of this flow was described qualitatively by VT who examined both the deep ($H > d$) and shallow ($H < d$) flow regimes. For reasons already discussed the present study focuses solely on the latter regime.

Over a wide range of values for the flux Q and fluid depths $H < d$, the core flow is observed to consist of a constant number (> 1) of stable mesovortices. The vortices propagate along an evolving curvilinear shear layer that intermittently spawns smaller vortices which then merge with the primary ones or get torn apart. Detailed measurements of the velocity field were not available at the time VT performed their experiment, but the number of mesovortices observed by them was typically less than the wavenumber of the original instability that produced them. A similar phenomenology has been observed in unforced two-dimensional numerical simulations for sufficiently thin initial vortex rings (Schecter *et al.* 1999; Kossin & Schubert 2001, e.g. their figures 4 and 9). For the range of aspect ratios and flow rates used here one observes four stable mesovortices without the upper lid.† The reverse flow is essential in this experiment for the maintenance of the multiple vortices. If the lower vessel is detached, as in the experiment of Whitehead & Porter (1978), a reverse flow cannot be formed and at all stages in the evolution of the flow a single vortex is observed.

To create an inflowing boundary layer underneath the free surface the upper lid is introduced (see figures 3*a* and 5*c*). Similar to the lower boundary layer, the tangential velocity is brought to rest along the bottom of the upper lid by the no-slip boundary condition. This enables the radial pressure gradient, that is in cyclostrophic balance with the tangential velocity of the bulk flow, to accelerate fluid toward the axis of symmetry. For a given volume flux, the width of the upper lid is empirically chosen to give an upper-layer inflow velocity in the desired proportion to the upper-layer tangential velocity. Further discussion of this point is given below. The experimental flow above the lower inflow layer then approximates the hurricane eye/eyewall flow in the lower troposphere when viewed 'upside down'.

For the geometrical parameters chosen and for the values of volume flux employed the free surface is nearly flat. Since accurate velocity measurements of the upper-level inflow layer using PIV methods are not possible with a strongly curved free surface, a flat surface is a desirable feature. Gravity then plays a negligible role in the dynamics of the experimental flow (Batchelor 1967) and the flow is essentially governed by the 'dynamic pressure' force. This aspect of the experiment is somewhat unlike that of a real hurricane whose dynamic pressure fluctuations on the vortex scale are more hydrostatically constrained (Shapiro & Montgomery 1993; Smith 1980). These differences notwithstanding, the horizontal core flows are similar.

For the remainder of this study we fix the volume flow rate Q equal to $120\,\mathrm{ml\,s^{-1}}$. This choice, in conjunction with the geometrical set up described above, constitutes our benchmark experiment. We do not report specific results using smaller or larger values of Q since no qualitative change in the flow was observed. The specific value of $120\,\mathrm{ml\,s^{-1}}$ was chosen based on the desire to attain a sufficiently high characteristic Reynolds number in the core region ($Re = VL/\nu \approx 7000$) while simultaneously producing a minimal distortion of the free surface associated with the parent vortex and mesovortices. The latter is tantamount to assuming a small external Froude number (i.e. $V/\sqrt{gH} \ll 1$, where g is gravity). Here V is the maximum tangential velocity

† For a summary of our preliminary results without an upper lid, see http://eliassen.atmos.colostate.epsdu: 'experimental vortex dynamics' and 'modeling the mesovortices at the hurricane eye'.

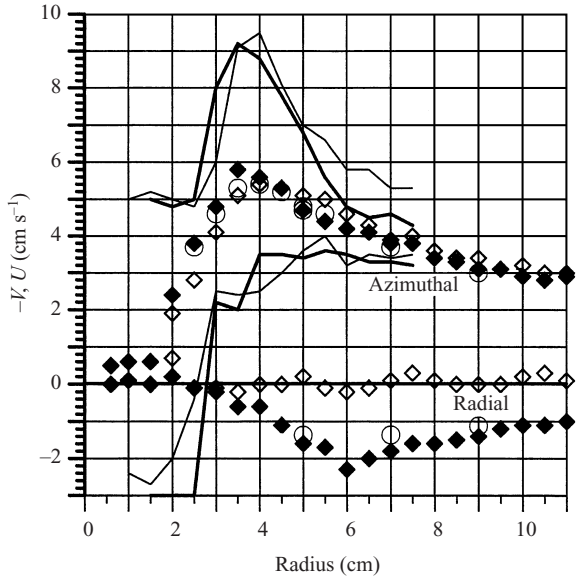

FIGURE 6. Measured tangential and radial velocities for benchmark experiment with $Q = 120\,\mathrm{ml\,s^{-1}}$ and $H = 4\,\mathrm{cm}$. Plotted are minus tangential velocity $-V$ and radial velocity U as a function of radius from the centre of the apparatus. ◆, Azimuthal and temporal average of minus the tangential velocity and radial velocity at $z = 3.5\,\mathrm{cm}$ (upper boundary layer); ◇, azimuthal and temporal average of minus the tangential velocity and radial velocity at $z = 2.0\,\mathrm{cm}$ (middle level); ○, azimuthal, temporal, and boundary-layer average of upper boundary-layer tangential and radial velocity. Dark curve denotes minima and maxima of the tangential velocity around the circumference at $z = 3.5\,\mathrm{cm}$. Light curve denotes minima and maxima in the tangential velocity around circumference at $z = 2.0\,\mathrm{cm}$.

measured ($\approx 9\,\mathrm{cm\,s^{-1}}$), L is the diameter of the vortex core region bounded by the RMW (8 cm), and ν is the kinematic viscosity of water at room temperature ($0.01\,\mathrm{cm^2\,s^{-1}}$).

Figure 6 shows measured velocities derived from single-frame multi-pulse images in horizontal planes for the benchmark experiment (see § 7 for details). Open diamonds denote the azimuthal mean tangential velocity and azimuthal mean radial velocity at $z = 2\,\mathrm{cm}$ from the bottom of vessel 1 as a function of radius from the centre of the apparatus. Solid diamonds denote the corresponding azimuthal mean tangential and radial velocity at $z = 3.5\,\mathrm{cm}$ (midpoint in the upper boundary layer, figure 5*c*). The azimuthal variability of the tangential velocity at $z = 2.0\,\mathrm{cm}$ and $z = 3.5\,\mathrm{cm}$ is displayed using, respectively, light and dark curves. These data show the maxima and minima tangential velocity (within 0.5 cm radial bins) around the circumference at each radial station. The approximate two-dimensionality of the mean and eddy components of the tangential velocity is striking.

Open circle data in figure 6 denote the azimuthal mean and boundary layer average tangential and radial velocities at selected radial stations. The boundary layer average is calculated by measuring the horizontal velocity at several heights within the upper boundary layer and integrating over the depth of the boundary layer ($\approx 1\,\mathrm{cm}$, figure 13). The velocity data at $z = 3.5\,\mathrm{cm}$ are clearly representative of the boundary layer average. The ratio of peak mean tangential velocity to peak mean radial velocity is approximately 2.5.

To suggest that the azimuthal and temporal mean of the experimental flow is similar to a real hurricane, observations of the corresponding mean inflow structure

are required. Unfortunately, the low-level inflow structure of a mature hurricane over the open ocean is the least documented compared to the azimuthal flow. The ratio of peak-mean tangential to peak-mean radial velocity in the inflow layer of an intense hurricane over the open ocean is generally thought to be greater than 2. Boundary layer observations are more prevalent for landfalling hurricanes (e.g. Powell 1982, 1996; Wurman & Winslow 1998), but these are not directly applicable to the current work because of strong spatial variations in the surface drag coefficient from open water to land. Airborne dual-Doppler data obtained by NOAA/AOML's Hurricane Research Division (e.g. Reasor *et al.* 2000) are not suitable either since the Doppler method does not accurately 'see' below $z \approx 1\,\mathrm{km}$ due to sea clutter (for a summary of airborne radar methods, see e.g. Houze 1993.) One must look elsewhere for observations of the azimuthal mean boundary layer inflow structure.

Assembling data from reconnaissance missions into Pacific typhoons at approximately 1000 ft. flight altitude above sea level, Hughes (1952) presented a composite low-level tangential and radial velocity profile of a stationary and moving typhoon. The characteristic inflow structure for a stationary typhoon was later confirmed for Atlantic hurricanes by Malkus & Riehl (1960) using flight-level and ship data gathered in Hurricanes Carrie (1957) and Daisy (1958). With a more extensive data set based on Pacific and Atlantic reconnaissance flights, Gray (1979) and Frank (1984) presented a low-level inflow structure consistent with the inflow data of Malkus & Riehl (1960). Thus for the present purpose the data from Hughes (1952) and Malkus & Riehl (1960) are believed sufficient. Figure 7 summarizes the observed low-level tangential and radial velocity profiles from Hughes (1952) and Malkus & Riehl (1960). Pertinent to our work is a ratio of maximum-mean tangential velocity to maximum-mean radial velocity between 2 and 3. Idealized axisymmetric hurricane numerical models (Shapiro 1983, §2; and Emanuel 1995) furnish a similar ratio of maximum-mean tangential to maximum-mean radial boundary layer velocities (see figure 8). The experimental ratio of 2.5 is thus consistent with what is known about the ratio of mean tangential velocity to mean radial velocity just outside the RMW in hurricanes.

An additional check on the similarity of the experimental flow to the eye/eyewall region of a real hurricane is furnished by considering the radius-to-width ratio of the azimuthal mean vorticity annulus that constitutes the curvilinear shear layer bordering the eye and eyewall region. If we adopt as a rough guide to the continuous problem the simplified three-region uniform-vorticity model of Michalke & Timme (1967) then the linear instability characteristics for the case of purely two-dimensional flow can be reduced to a two-parameter space (δ, γ), where δ is the ratio of inner and outer radius of elevated vorticity, and γ is the ratio of inner vorticity to the areal average vorticity within the RMW of the azimuthal mean vortex (Schubert *et al.* 1999). In terms of δ, the radius-to-width ratio is then $\delta/(1-\delta)$. Observations of several intense hurricanes suggest that the radius-to-width ratio varies between 0.5 (Kossin & Schubert 2001, figure 1*a*) and 5 (Kossin & Schubert 2001, figure 1*c*). If to estimate δ we use the experimentally measured azimuthal mean tangential velocity distribution at $z = 3.5\,\mathrm{cm}$ (figure 6) we obtain $\delta = 1.5/3.5 = 0.425$ and thus a radius-to-width ratio of 0.75. This is clearly in the range of observed values.†

† We have not undertaken here a detailed study of the dependence of the asymmetric flow on this radius-to-width ratio. Given the observed variation of this quantity between storms (and even within a storm's lifecycle), a future experimental study devoted solely to this issue would be of considerable practical and theoretical interest.

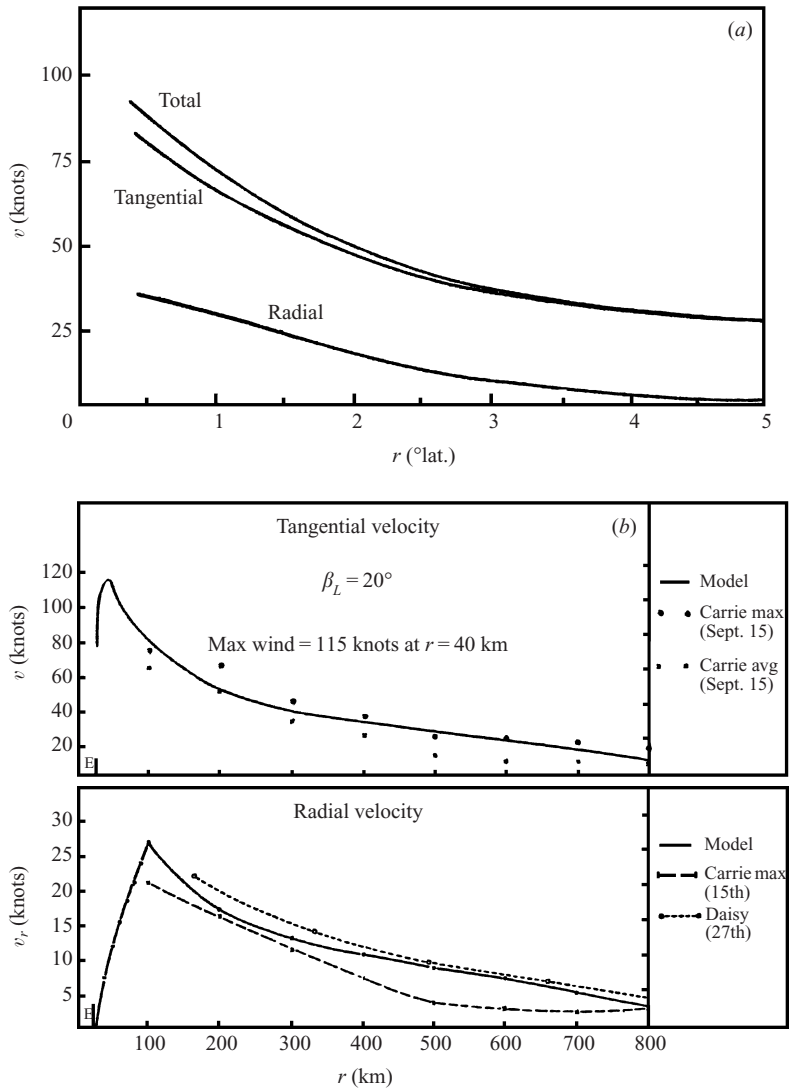

FIGURE 7. Observed low-level radial profiles of mean tangential and mean radial velocity in typhoons and hurricanes. (*a*) Composite radial profile from reconnaissance flights into Pacific typhoons at an altitude of approximately 1000 ft. Adapted from Hughes (1952). (*b*) Radial profiles from Atlantic Hurricanes Carrie (1957) and Daisy (1958). (Sign of radial inflow reversed for convenience.) Radial inflow data based on ship obervations. Adapted from Malkus & Riehl (1960).

5. Flow visualization

Visualization experiments were carried out using blue ink at various locations in the flow. The laser from the PIV was also used for illuminating the flow by using horizontal and vertical light sheets. Figure 9 shows photographs of ink visualizations for the benchmark flow. Horizontal and vertical scales are depicted in figure 9(*a*) and the centre is indicated by the vertical dashed line. Ink was injected into the flow using a syringe. Figure 9(*a*) shows a side view of the two primary mesovortices. The mesovortices reside inside the RMW of the mean flow depicted in figure 6. The quasi-two-dimensional nature of the horizontal flow within and near the mesovortices

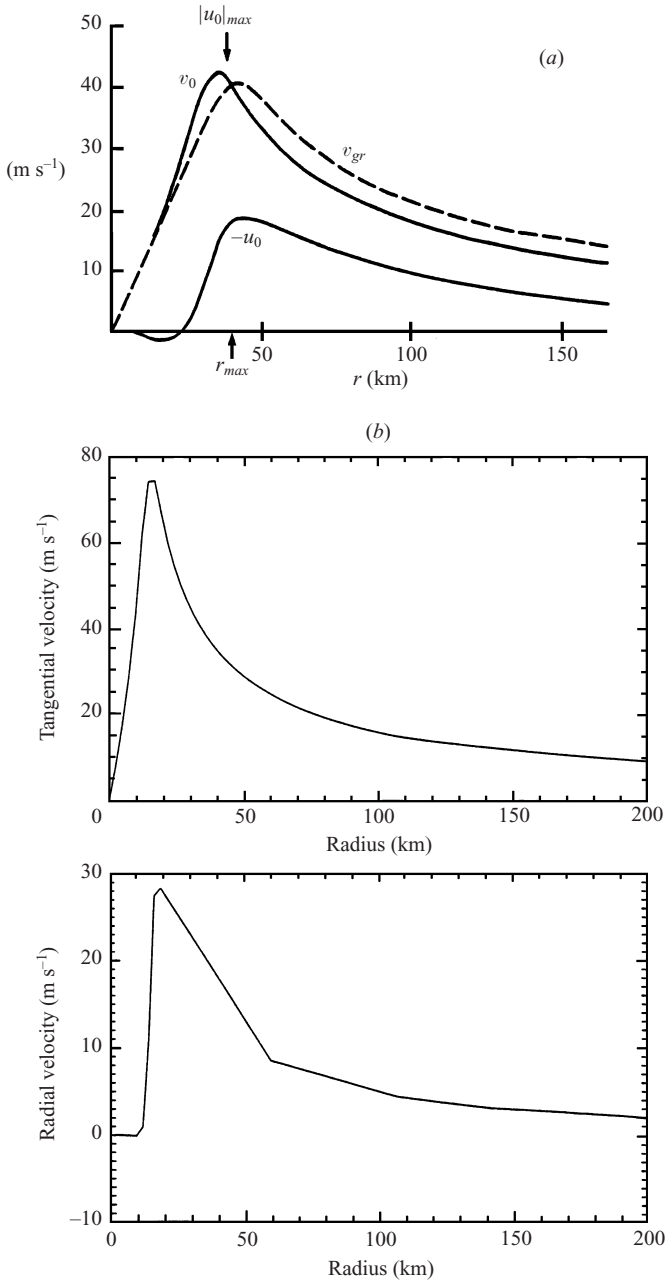

FIGURE 8. Predicted low-level radial profiles of mean tangential and mean radial velocity using idealized axisymmetric hurricane numerical models. (*a*) 'Slab' boundary layer prediction of Shapiro (1983, his figure 4). (*b*) Hurricane model prediction of Emanuel (1995) assuming boundary layer quasi-equilibrium. Tangential and radial velocity data displayed at $z = 540$ m. (This model simulation uses parameters of control experiment with SST = 27 C. See Emanuel 1995 for details.)

is striking (cf. figure 6). The black disk-like image on the bottom of vessel 1 in figure 9(*a*) is the circular orifice, but the hole cannot be seen from this vantage point. Figure 9(*b*) is a plan-form view of the core flow (looking from above), with the clear hole in the centre now visible. Two primary vortices as well as two secondary

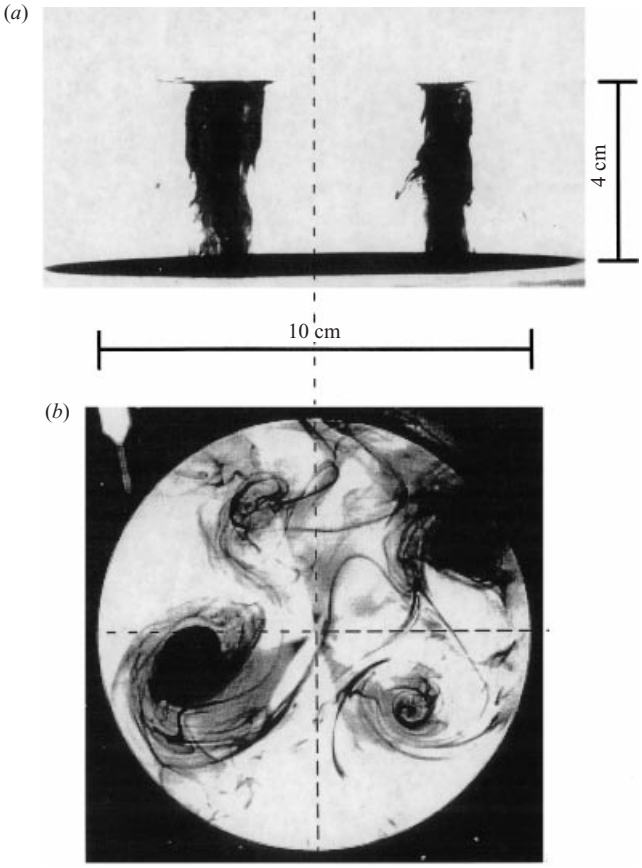

FIGURE 9. Ink visualization of benchmark flow. (*a*) Side view. (*b*) Plan view looking from above. From (*a*) and figure 6, it is evident that the horizontal flow is approximately two-dimensional ('rotationally stratified'). Primary and secondary vortices are evident in (*b*).

vortices are evident. The primary vortices are located at a mean radius of 2.5 cm and propagate around the centre of circulation with an approximately constant period of 5.5 s. This period is slightly less than the 5.8 s turnaround time of the mean tangential flow at $z = 2$ cm and $r = 2.5$ cm. Unlike the primary mesovortices which are observed to be stable and robust coherent structures, the secondary mesovortices are observed to form along the evolving shear layer and to be unstable (lifetime less than one minute), ultimately merging with the primary vortices or being torn apart.

Figure 10 shows a photograph of the horizontal flow when illuminated with the horizontal laser sheet at $z = 3.5$ cm. The image nicely illustrates the principal features of the experimental flow. The silvered particles embedded in the flow produce beautiful streak lines. The nearly stagnant upwelling flow in the centre is visible as well as the primary curvilinear shear layer bordering the interior and exterior region of the core flow. Two primary mesovortices are clearly evident along with two secondary mesovortices. Just outside the primary shear layer, curved flow features (filaments) make arcs around the core flow and spiral inward in a clockwise ('cyclonic') sense. The filaments are observed to elongate in time. The streaklines near the filaments suggest that the filaments possess both cyclonic vorticity and horizontal convergence. The filaments appear qualitatively similar to sheared vortex waves (Melander, McWilliams

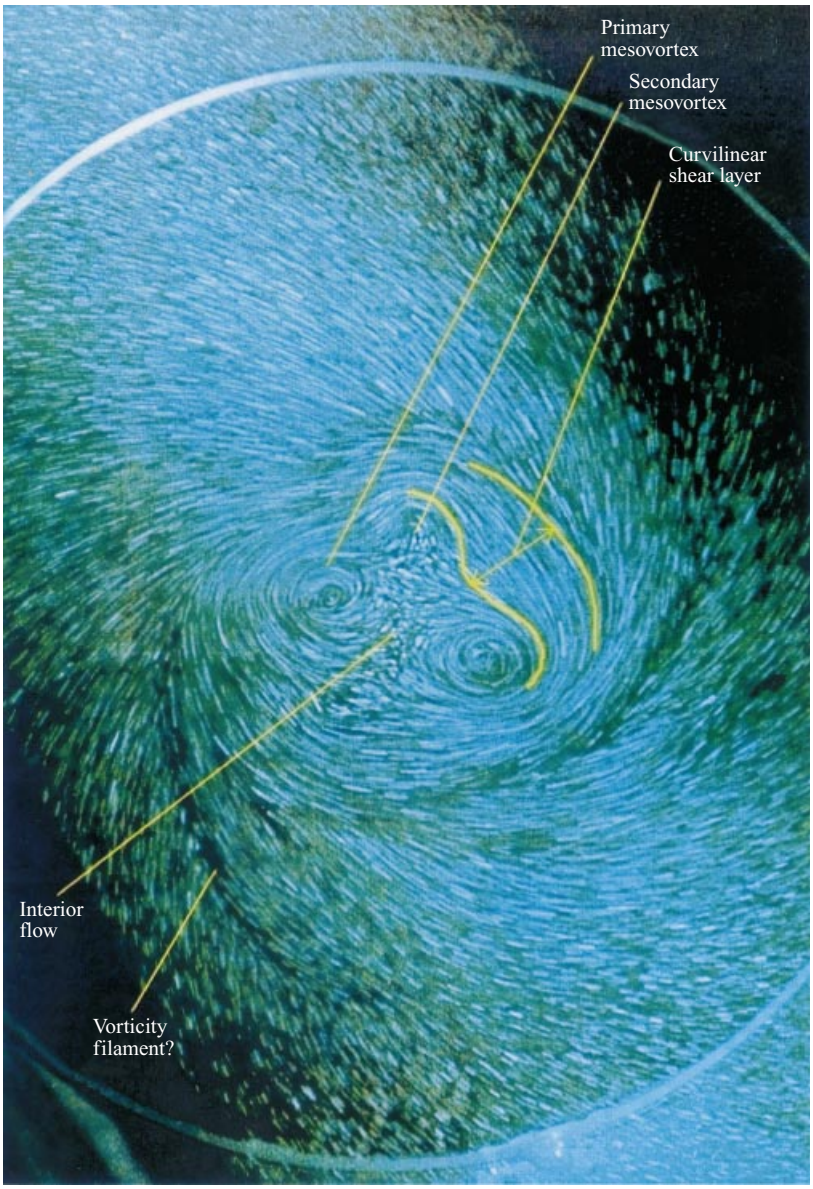

FIGURE 10. Plan-view of benchmark flow looking from above using laser and silvered particles to illuminate the flow at $z = 3.5$ cm. Noteworthy are the two primary mesovortices and secondary vortices in the central region, and the spiral-like filaments outside the core that spiral 'cyclonically' inward.

& Zabusky 1987; Guinn & Schubert 1993; Montgomery & Kallenbach 1997; Chen & Yau 2001; Wang 2002*a*, *b*), but a thorough diagnosis of their structure and dynamics in this experiment awaits more detailed measurements with the PIV.

6. PIV setup

Velocity measurements were obtained using a particle image velocimeter (PIV) (see figure 11). A description of the PIV method can be found, for example, in

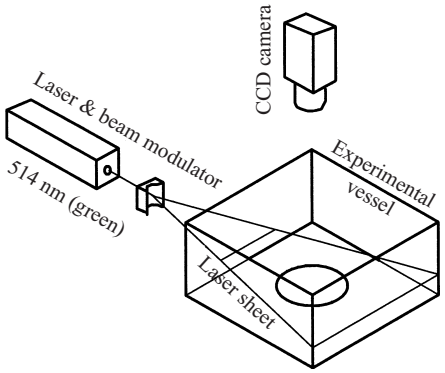

FIGURE 11. Schematic of PIV setup.

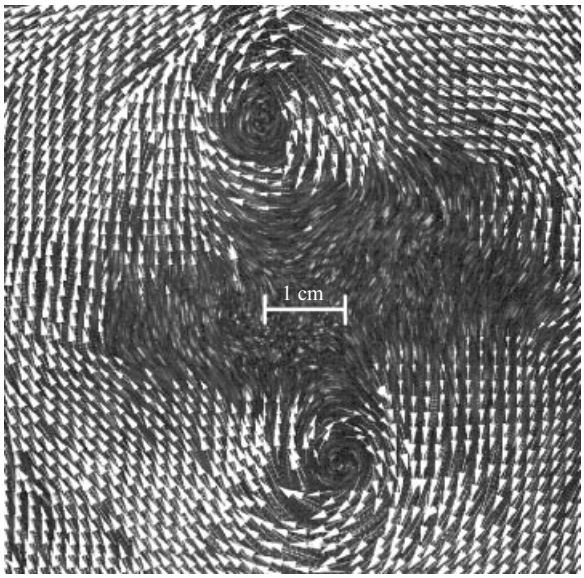

FIGURE 12. Typical PIV image with corresponding horizontal velocity field overlaid on image at $z = 3.5$ cm. Separation between laser pulses is 40 ms.

Adrian (1991). An argon ion laser Innova70 (power up to 4 W) with Bragg Cell beam modulator was used as a light source (wavelength of 514 nm). Pulses with a typical time separation from 4 to 80 ms and a duration of 20% were used. A concave cylindrical lens was used to form the laser sheet. For certain experiments a focusing spherical lens was used to make the laser sheet thickness of order 0.1 mm. To measure the horizontal velocity at different depths in the flow, the laser sheet was positioned horizontally at different distances from the bottom of the vessel. To measure the transverse (secondary) flow, the laser sheet was positioned vertically through the plane of symmetry. Silvered hollow particles with diameters of approximately 20 μm and density of approximately $1.2\,\mathrm{g\,cm^{-3}}$ were used for flow diagnostics. Grey-scale 8-bit images were captured with a Kodak Megaplus CCD camera with a viewfield of 1034×1316 pixels. The velocity field was calculated using Insight 3.0 software (By TSI Inc.). An example of the measured flow near the centre at $z = 3.5$ cm is shown in figure 12. In this case the separation between pulses was 40 ms in order to accurately resolve the flow in the central area.

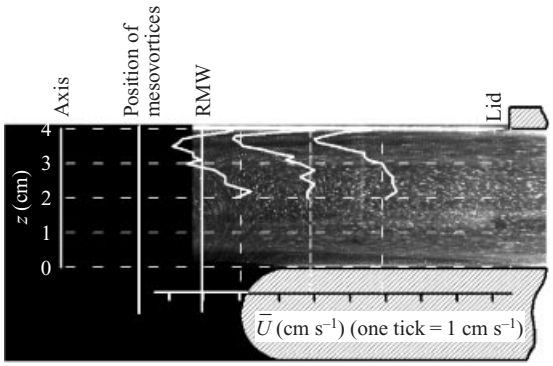

FIGURE 13. Typical PIV image of transverse flow overlaid on corresponding mean radial velocity as a function of z at $r = 5$, 7 and 9 cm in the upper boundary layer. Sideview illuminated by vertical laser sheet of 5 mm thickness. Separation between laser pulses is 40 ms. Azimuthal and temporal averages of data similar to those of figure 6.

Because of the resolution limits inherent in the PIV setup it was not possible to obtain accurate velocity measurements for the mesovortices and exterior flow simultaneously. For this purpose separate images with resolution of approximately 70, 140, and 320 pixels cm^{-1} were obtained. The first image was used to measure the velocity field far from the vortex core region, while the third image was used to resolve the velocity field inside the mesovortices. The second image was used for the intermediate region and as a consistency check on the first and third images. The velocity fields from each image were then overlaid on the same graph to create, e.g., figures 6 and 15.

7. Velocity measurements

A side view of the benchmark flow through the vertical plane of symmetry is presented in figure 13. Along the top of the figure are pertinent reference radii, namely, the axis of symmetry ($r = 0$), the mean radial position of the primary mesovortices ($r \approx 2.5$ cm), the RMW ($r \approx 4$ cm), and the interior radius of the upper lid ($r = 12.5$ cm). Vertical distance is indicated along the axis of symmetry. The depth of each (inflow) boundary layer is approximately constant at 1 cm between $r = 12.5$ cm and $r \approx 5$ cm. Despite their vertical proximity, the two boundary layers are observed to be approximately independent. Essentially the same primary and secondary mesovortex structures are observed in another experiment using the same flow rate (120 ml s^{-1}), but with twice the fluid depth (8 cm).

Figure 13 shows the azimuthal and temporal mean radial velocity $\bar{u}$ as a function of depth in the upper-half of the flow at three radial stations ($r = 5$, 7, 9 cm) for the benchmark experiment. The radial velocity distributions are overlaid on a single-frame multi-pulse image of the transverse flow. The separation between the laser pulses is 40 ms and the vertical laser sheet is ≈ 5 mm thick. The distribution of the azimuthal mean radial velocity derived from the vertical image indicates a peak inflow velocity of $\bar{u} \approx 2.4$ cm s^{-1} at $r = 6$ cm and $z \approx 3.75$ cm (cf. figure 6). There is essentially no mean inflow/outflow outside the upper and lower boundary layers. The general structure of the upper and lower boundary layer flow is approximately invariant among images, but the vertical velocity radially near the RMW is unsteady and more intermittent than suggested by this image.

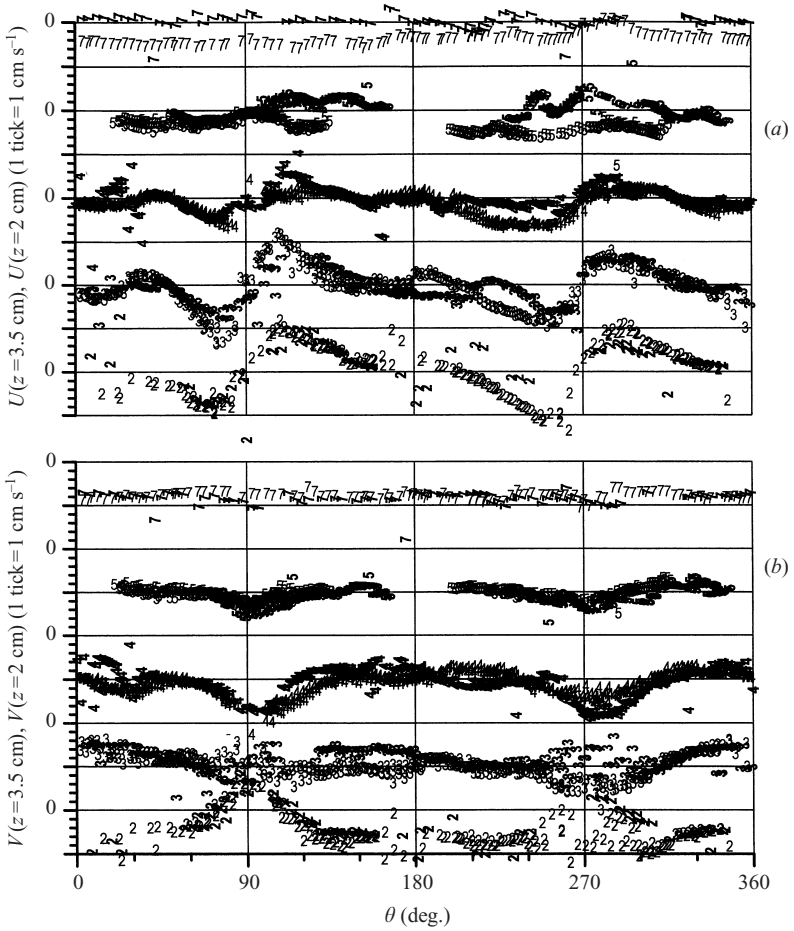

FIGURE 14. Angular dependence of radial (a) and tangential (b) velocities at different radii for the benchmark flow. Velocities in the radial intervals (1.75, 2.25) cm, (2.75, 3.25) cm, etc. are presented. 90° and 270° angles correspond to the primary mesovortices. Data labels correspond to the radius bin (cm). Vertical labels correspond to data at $z = 3.5$ cm. 90°-counterclockwise-rotated labels correspond to data at $z = 2$ cm.

Figures 14(a) and 14(b) show the azimuthal dependence of the measured radial and tangential velocity at different radii from the axis of symmetry. The velocity data are shown for two heights in the flow, one at $z = 3.5$ cm (midpoint of upper boundary layer) and the other at $z = 2$ cm (middle level). The data are binned into radial intervals of width 0.5 cm centred at $r = 2, 3, 4, 5, 7$ cm. The data are shifted along the horizontal axis so the centre of one of the primary mesovortices corresponds to 90° of azimuthal angle. The second mesovortex typically resides near 270° azimuth. For both heights, one single-frame multiple-pulse image is taken in order to supply the data out to $r = 5$ cm radius. The corresponding data at $r = 7$ cm are obtained with a second image to cover the outer-core flow. The two data sets yield consistent velocity fields.

In the central part of the core flow ($r \leqslant 2$ cm) the radial velocity is comparable to the tangential velocity at both heights. The upwelling velocity occurs mainly in the central region (not shown) and is observed to be approximately 1 cm s^{-1}. Ink visualizations suggest that the downwelling velocity is localized spatially in spiral curtains around

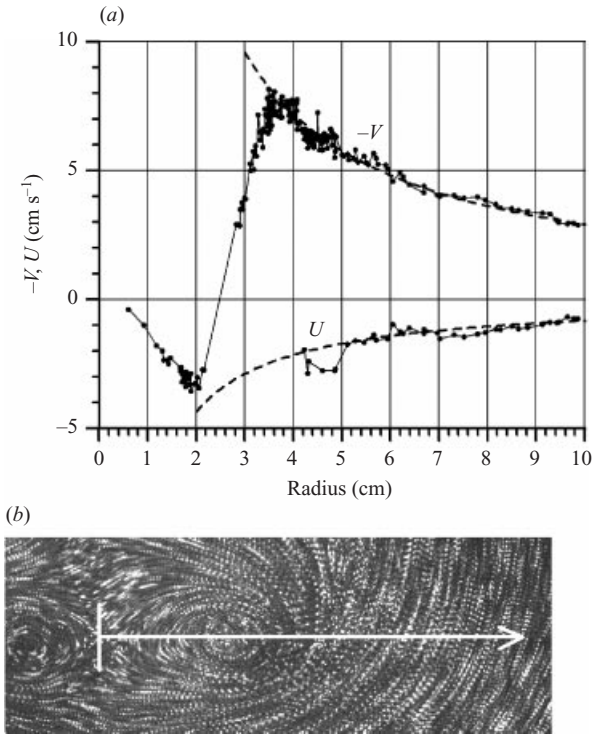

FIGURE 15. (*a*) Radial profile of minus tangential and radial velocity at $z = 3.5\,\text{cm}$ along the line shown by the white arrow. Dotted lines correspond to a best-fit $1/r$ dependence for both tangential and radial velocity. (*b*) Corresponding PIV image at $z = 3.5\,\text{cm}$. See text for details.

the mesovortices (not shown) having a magnitude locally of approximately $4\,\text{cm s}^{-1}$. Farther out in the core flow ($r \leqslant 5\,\text{cm}$) the radial velocity vanishes at azimuths where the tangential velocity reaches its maximum. This is expected for a flow containing vortices. While the near-coincidence of velocity maxima between the two height levels is suggestive of an approximately two-dimensional horizontal flow, strictly speaking, our procedure used to orient the data prevents such a conclusion. If the mesovortices were helical, for example, figure 14 would not change. The ink visualization of § 5, however, confirms that the horizontal core flow is approximately two-dimensional. The tangential velocity data show two distinct maxima near 90° and 270° azimuth in association with the two primary mesovortices. At $z = 3.5\,\text{cm}$ the local tangential velocity attains a peak value of approximately $9.0\,\text{cm s}^{-1}$ (50% greater than the azimuthal mean at this level). The local tangential velocity at $z = 2\,\text{cm}$ attains a slightly larger peak value of approximately $9.5\,\text{cm s}^{-1}$ (70% greater than the azimuthal mean at this level). In the outer-core region ($r \geqslant 5\,\text{cm}$) the radial velocity is much smaller than the tangential velocity except in the boundary layers. Unlike for $z = 3.5\,\text{cm}$ where a mean inflow is evident for $r \geqslant 5\,\text{cm}$, at $z = 2\,\text{cm}$ there is approximately no mean inflow at these radii.

Figure 15 shows a radial profile of the measured tangential and radial velocity from $r = 0$ to $r = 10\,\text{cm}$ at a height of $z = 3.5\,\text{cm}$ (upper boundary layer). The sign of the tangential velocity in (*a*) has been reversed to facilitate comparison with hurricane observations. The velocity data are for the radial segment passing through the centre of the mesovortex to the right of the symmetry axis, indicated by the white arrow. The data are derived from single-frame multi-pulse images, the largest of which is

shown below the radial plot. The velocity resolution limits imposed by the PIV setup prevented obtaining accurate velocity measurements of the mesovortices and exterior flow simultaneously (see § 6). To circumvent this difficulty three separate images were obtained with increasing resolution in order to resolve the velocity field inside the mesovortex. The velocity data from each of these images were then overlaid on the same graph to create the plot shown. The velocities bordering each region are in approximate agreement, confirming the consistency of this procedure.

Two features in figure 15 are noteworthy. The first is the approximate agreement between the $1/r$ profiles (dashed) and the measurements. The discrepancy between measurements and the $1/r$ decay is greatest for the tangential and radial velocity near the visible outer edge of the mesovortex ($r = 4.5$ cm). The second is that the local tangential velocity exceeds the azimuthal mean of the swirling flow of figure 6 by approximately 40%. That the experimental tangential and radial velocity both decay as $1/r$ outside the RMW is not surprising since for $r < 12.5$ cm the upper-level boundary layer flow has no angular momentum sink and the orifice acts like a mass sink to the inflowing fluid. The relatively rapid radial decay with radius outside the RMW is unlike that observed in real hurricanes where the tangential and radial velocities decay more slowly than $1/r$ (e.g. figure 7; Riehl 1963; Pearce 1992; and Kossin & Schubert 2001, their figure 1).

Because of the practical implications of the results we compare the intensity of the experimental mesovortices to the parent vortex that supports them. To estimate the ratio of the horizontal velocity within the primary mesovortices to the azimuthal and temporal mean tangential velocity around the centre of circulation let us focus on the upper boundary layer flow ($z = 3.5$ cm). The data of figure 15 show a difference in tangential velocity of approximately $11.5\,\mathrm{cm\,s^{-1}}$ across one of the mesovortices. The region between the tangential velocity maximum and minimum is the core of the mesovortex and the diameter of the core is approximately 1.5 cm. In the core region of the mesovortex the fluid is in approximate solid body rotation. If the midpoint between the tangential velocity maximum and minimum is defined as the centre of the mesovortex ($r = 2.8$ cm) then the vortex translates with a tangential velocity of approximately $2\,\mathrm{cm\,s^{-1}}$. Subtracting this velocity from the maximum and minimum tangential velocity yields an average maximum tangential velocity V_m for the mesovortex of approximately $5.75\,\mathrm{cm\,s^{-1}}$ (approximately the same as the maximum azimuthal and temporal mean tangential velocity at this z level). The vorticity of the mesovortex core ζ_m can be estimated using the equation $\zeta_m = 2V_m/R_{core}$, where R_{core} denotes the core radius of the primary mesovortex. From figure 15, $R_{core} \approx 0.75$ cm and therefore $\zeta_m \approx 15\,\mathrm{s^{-1}}$. A similar value for ζ_m was obtained by observing the orbital period of small styrofoam particles placed within the mesovortices. Given the maximum vorticity of $4.4\,\mathrm{s^{-1}}$ for the azimuthal mean flow at this z-level (see figure 16), the ratio of mesovortex vorticty to mean vorticity is then roughly three to one.

8. Stability analysis

The robustness of the primary mesovortices in the presence of a relatively strong transverse flow through the core of the parent vortex is somewhat surprising. Why there are only two of them is particularly intriguing. Competing theories have been offered previously to explain the multiple vortex phenomenon in two-celled vortex flows (VT; Lugovtsov 1982; Gall 1983; Rotunno 1984). Unlike the strictly two-dimensional 'free-decay' laboratory and numerical experiments of Jin & Dubin (1998), Schecter *et al.* (1999), and Kossin & Schubert (2001) that examine the relaxation

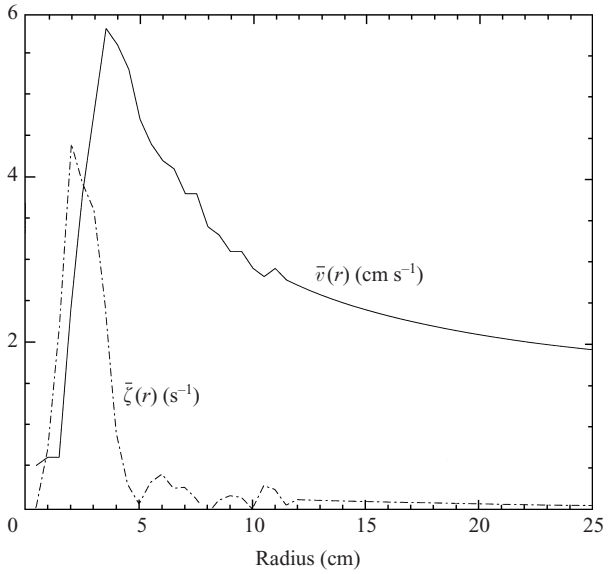

FIGURE 16. Mean tangential velocity $-\bar{v}$ and corresponding relative vorticity $-\bar{\zeta}$ derived from experimental data of figure 6 at $z = 3.5$ cm.

of initial vorticity distributions into 'vortex crystals', the present experimental flow is maintained by a secondary circulation. We know nothing about the statistical mechanics of two-celled vortex flows.

As far as we are aware there are no general analytical results concerning the three-dimensional linear stability of a homogeneous vortex flow possessing a mean primary and mean secondary circulation $(\bar{u}(r,z), \bar{v}(r,z), \bar{w}(r,z))$. Here, $(\bar{u}, \bar{v}, \bar{w})$ denote the azimuthal and temporal mean radial, tangential, and vertical velocity, respectively, of the basic-state vortex flow. Considering for the moment strictly tangential flow $(0, \bar{v}(r), 0)$, Rayleigh (1916) proved stability to inviscid axisymmetric (r,z) perturbations provided $I^2 = r^{-3}\partial(r^2\bar{v}^2)/\partial r > 0$, where I^2 represents the centrifugal (inertial) stability of the mean tangential flow. Howard & Gupta (1962) generalized this axisymmetric stability criterion to include the radial shear of the vertical velocity through the vortex; they showed that flows $(0, \bar{v}(r), \bar{w}(r))$ are stable to axisymmetric (r,z) perturbations provided $I^2(\mathrm{d}\bar{w}/\mathrm{d}r)^{-2} > 1/4$. For small-scale helical modes Leibovich & Stewartson (1983) derived a sufficient condition for the instability of a columnar vortex, namely, $[\bar{v}\mathrm{d}\bar{\Omega}/\mathrm{d}r][\mathrm{d}\bar{\Omega}/\mathrm{d}r\,\mathrm{d}\overline{M}/\mathrm{d}r + (\mathrm{d}\bar{w}/\mathrm{d}r)^2] < 0$, where $\bar{\Omega} = \bar{v}/r$ is the azimuthal mean angular velocity and $\overline{M} = r\bar{v}$ is the azimuthal mean angular momentum per unit mass. After transforming the perturbation equations into a local coordinate system parallel to the helical streamlines of the flow, Emanuel (1984) showed that these helical instabilities are essentially inertial (centrifugal) in character.

Let us consider first the question of axisymmetric stability of the experimental flow. Though we have not measured accurately the azimuthal mean vertical velocity, video recordings of the transverse flow illuminated with the silvered particles allow us to estimate whether Howard & Gupta's (1962) sufficient criterion for axisymmetric stability is violated. Considering the region just inside the RMW of the azimuthal mean flow where the radial derivative of vertical velocity is near a maximum, figure 16 indicates that $I^2 \approx 4^2\,\mathrm{s}^{-2}$. The video recordings of the transverse flow (not shown) suggest that $\partial\bar{w}/\partial r \approx (2\,\mathrm{cm\,s}^{-1})/(1\,\mathrm{cm}) = 2\,\mathrm{s}^{-1}$. We then obtain $I^2(\partial\bar{w}/\partial r)^{-2} \approx 4 \gg 1/4$. The

azimuthal mean flow should thus be stable to axisymmetric perturbations. (In a real hurricane the square of the radial shear of the vertical velocity is small compared to the centrifugal stability of the primary swirling flow and hence $I^2(\partial\bar{w}/\partial r)^{-2} \gg 1/4$.)

The question of helical instability, and more generally three-dimensional instability, of the experimental flow is more complex. Figure 9(*b*) suggests (and video recordings confirm) the existence of small-scale helical structures within and just outside the core of the mesovortices. At present we do not possess sufficient data of the vertical velocity field to determine whether these helical structures are the result of the Leibovich–Stewartson instability or sheared vortex waves with vertical structure that are generated by the vortex distortion induced by the near-core flow (Montgomery & Kallenbach 1997; Bassom & Gilbert 1999; Schecter *et al.* 2000; Möller & Montgomery 2000). On larger scales, however, it is clear that the interior flow is dominated by the mesovortices. The approximate two-dimensionality of the horizontal flow (cf. figure 6 and figure 9) suggests that a two-dimensional (Kelvin–Helmholtz) stability analysis of the observed mean curvilinear shear flow should be a valid first step towards characterizing the dominant asymmetric modes of the two-celled vortex flow.

Neglecting the secondary circulation and recalling that the characteristic Reynolds number is reasonably large, the two-dimensional stability model employs the inviscid non-divergent vorticity equation linearized about a basic state of circular shear flow:

$$\frac{\partial\zeta'}{\partial t} = -\bar{\Omega}\frac{\partial\zeta'}{\partial\lambda} + \frac{\partial\psi'}{r\partial\lambda}\frac{\mathrm{d}\bar{\zeta}}{\mathrm{d}r}, \tag{1}$$

where $\bar{\zeta}(r) = \bar{v}(r)/r + \mathrm{d}\bar{v}/\mathrm{d}r$ denotes the basic state vorticity, $\zeta' = \zeta'(r,\lambda,t) = v(r)/r + \mathrm{d}v/\mathrm{d}r$ the perturbation vorticity, $\psi'(r,\lambda,t)$ the perturbation streamfunction, λ the azimuthal angle, and t the time. The perturbation vorticity and streamfunction are related by the Poisson relation $\zeta' = \nabla^2\psi'$. Basic state variables required in (1) are obtained from the azimuthal and temporal mean velocity data of figure 6 at $z = 3.5\,\mathrm{cm}$ of vessel 1 (upper boundary layer). It is straightforward to see that the mean tangential flow satisfies both Rayleigh's and Fjortoft's necessary condition for curvilinear shear instability (Gent & McWilliams 1986).

Normal-mode solutions to (1) for the perturbation streamfunction are sought in the form

$$\psi'(r,\lambda,t) = \mathrm{Re}(\hat{\psi}(r)\exp[\mathrm{i}(n\lambda - \nu t)]), \tag{2}$$

where Re denotes real part, $\hat{\psi}(r)$ is the eigen-streamfunction amplitude, n is the azimuthal wavenumber, and ν is the eigen-frequency. The eigen-streamfunction amplitude and eigenfrequency $(\hat{\psi}(r), \nu)$ are obtained using the finite difference formulation following Gent & McWilliams (1986). Eigensolutions with positive imaginary part ($\nu_i = \mathrm{Im}(\nu) > 0$) grow exponentially with time. Letting the real part of the frequency $\nu_r = \mathrm{Re}(\nu)$, the angular rotation rate of the eigenmode is ν_r/n, and its orbital period is $2\pi n/\nu_r$.

Figure 16 shows radial profiles of the mean tangential velocity $-\bar{v}(r)$ and mean vorticity $-\bar{\zeta}(r)$ at $z = 3.5\,\mathrm{cm}$ in vessel 1. A convention of 'counterclockwise flow' has been adopted. To minimize 'image charge' effects associated with the outer boundary, the mean tangential velocity has been extended to an outer radius by matching the data onto a $1/r$ profile beyond $r = 11\,\mathrm{cm}$ (cf. figure 6). An outer boundary of $r_{max} = 25\,\mathrm{cm}$, and an inner boundary of $r_{min} = 0.5\,\mathrm{cm}$ are used here. (Recall that the curved Plexiglas wall is at $r \simeq 36\,\mathrm{cm}$.) Because of the inaccuracy of the PIV measurement close to the centre (where the velocities are small), the mean vorticity is set to zero at the innermost boundary point r_{min}. The radial grid spacing employed

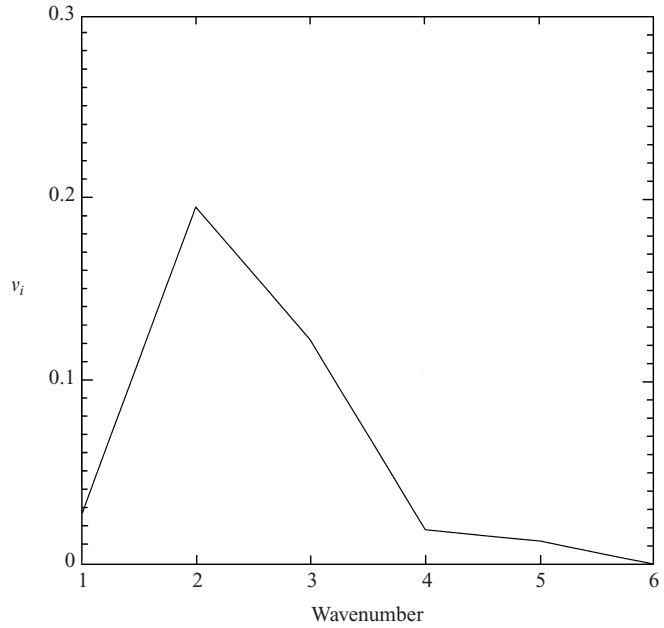

FIGURE 17. Two-dimensional most unstable growth rate (v_i) for each azimuthal wavenumber (n) as a function of n for the flow of figure 16. See text for details.

is $\delta r = 0.5\,\text{cm}$ (the resolution of the velocity data shown in figure 6). The principal results regarding the unstable eigenmodes have been verified to be robust if r_{min} is decreased to 0.01 cm, r_{max} is increased to 50 cm, or the resolution is doubled.

Figure 17 shows the predicted most unstable growth rates v_i as a function of azimuthal wavenumber for wavenumbers 1 to 6. The most unstable mode occurs at wavenumber 2 with a growth rate of approximately $v_i = 0.19\,\text{s}^{-1}$. The e-folding time for this mode is 5.2 s, slightly less than one turnaround time of the azimuthal mean flow at the RMW. The mode with the next largest growth rate occurs at wavenumber 2 (not shown in figure 17) and has a growth rate of $v_i = 0.17\,\text{s}^{-1}$. The real part of v for these two modes is found to be $v_r = 2.79\,\text{s}^{-1}$ and $v_r = 1.65\,\text{s}^{-1}$, respectively. The orbital period of these modes is then 4.5 s and 7.61 s, respectively. The observed rotation period of the mesovortices is approximately 5.5 s. While neither precisely matches the rotation period of the mesovortices, the orbital periods are comparable.

Figure 18 shows contour plots of the unstable vorticity eigenmodes for azimuthal wavenumber 2. Figure 18(a) shows the vorticity eigenmode with the largest growth rate, while the bottom plot shows the eigenmode with the next largest growth. The most unstable vorticity eigenmode has its maximum amplitude at $r = 2\,\text{cm}$. We recall that the primary mesovortices reside at a mean radius of $r = 2.5\,\text{cm}$.

In the context of the stability properties of two-celled vortex flows these results are interesting and justify brief discussion. It has been suggested previously, based on numerical simulations of the tornado chamber experiments of Ward (1972) and Church *et al.* (1977), that the multiple vortex phenomenon in tornado-like vortices depends essentially on both the radial shear of the tangential velocity and the radial shear of the axial velocity in the vortex core (Rotunno 1984, §4). Our calculation shows, however, that the two-dimensional stability model (radial shear of axial velocity neglected) yields a wavenumber 2 instability whose radial structure and phase speed are roughly consistent with the experimental observations of the primary mesovortices.

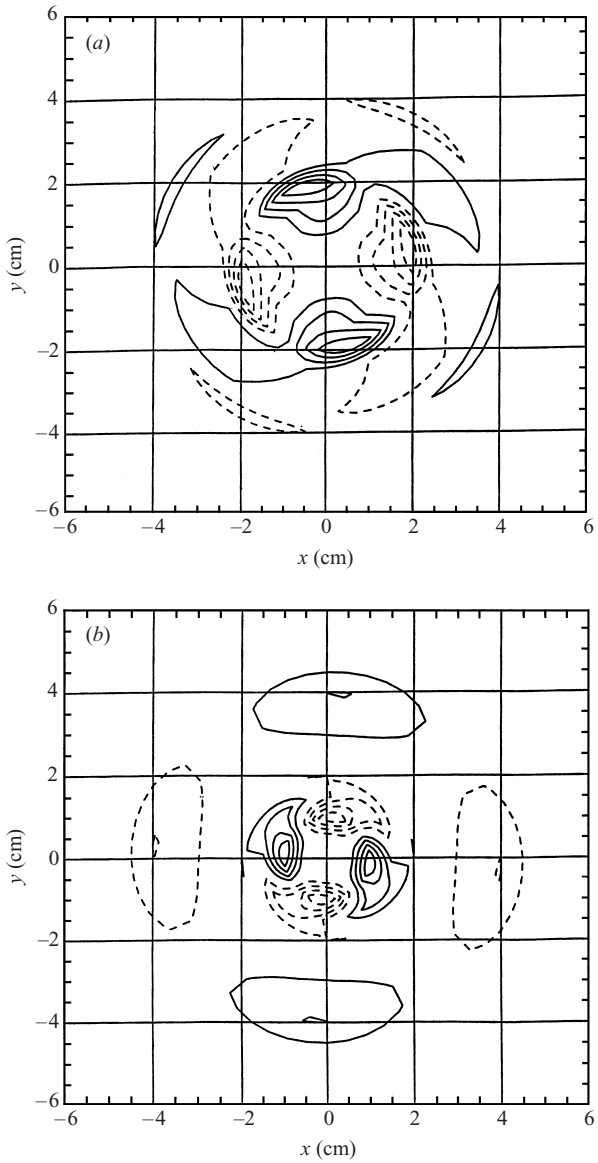

FIGURE 18. Two-dimensional unstable vorticity eigenmodes for the flow of figure 16. (*a*) Most unstable vorticity eigenmode ($v = 2.8\,\mathrm{s}^{-1} + \mathrm{i} \times 0.19\,\mathrm{s}^{-1}$, $n = 2$), where $\mathrm{i}^2 = -1$. (*b*) Next unstable vorticity eigenmode ($v = 1.65\,\mathrm{s}^{-1} + \mathrm{i} \times 0.17\,\mathrm{s}^{-1}$, $n = 2$). Recall that the amplitude scale is arbitrary in the linear stability problem. See text for details.

The three-dimensional stability analysis of Gall (1983) supports our two-dimensional stability predictions. Considering the multiple vortex phenomenon in tornadoes of various intensities, Gall examined the dependence of the three-dimensional unstable eigenmodes of a depth-independent mean vortex $(0, \bar{v}(r), \bar{w}(r))$ on the swirl ratio. The swirl ratio S is defined by

$$S = \frac{\Gamma r_0}{Q}, \tag{3}$$

where Γ is the horizontal circulation of the swirling flow, r_0 is the 'outer' radius,

and Q is the volume flow rate through the vortex. As S exceeded unity the two-dimensional (non-divergent) model (equation (1)) was found to furnish qualitatively quantitately correct approximations to the dominant unstable eigenmodes, growth rates and energetics for the horizontal core flow. For our benchmark experiment we take $r_0 = \mathrm{RMW}$, $\Gamma = 2\pi \times \mathrm{RMW} \times \bar{v}(\mathrm{RMW})$, and $Q = 60\,\mathrm{ml\,s^{-1}}$ (the upper inflow layer only) to obtain $S \sim 9 \gg 1$. (In a real hurricane $\Gamma \gg Q/r_0$, hence $S \gg 1$.) Gall's results together with the two-dimensional stability analysis hence suggest that the multiple vortex phenomenon and related large-scale features discussed in § 5 are governed by quasi-two-dimensional fluid dynamics (McWilliams 1985; Shapiro & Montgomery 1993).

The influence of the transverse flow on the two-dimensional eigenmodes constructed here, the impact of nonlinearity, and the dynamics of the small-scale helical structures are important topics that should be considered in forthcoming work.

9. Discussion and conclusions

The exchange of angular momentum between a hurricane's eyewall and eye by eddy processes is believed important from both thermodynamical and fluid dynamical viewpoints. Recent work suggests that this exchange occurs primarily through quasi-two-dimensional fluid dynamics (vortex waves, mesovortices, and vorticity mixing). Quantitatively, little is known, however, about all of these processes in hurricanes. To obtain further insight into the fluid dynamics of the hurricane eye/eyewall region, and hurricane mesovortices in particular, an 'upside down' hurricane simulator has been constructed to simulate the lower tropospheric flow near the eye of the storm. The experimental apparatus is a modification of that described previously by Vladimirov & Tarasov (1980) and uses a particle image velocimeter to obtain velocity measurements of the core flow of the vortex. The application and velocity measurements are new and the results furnish new insight into the dynamics of the multiple vortex phenomenon and the eye/eyewall flow of an intense hurricane.

The experimental apparatus is constructed so as to generate a mean boundary layer inflow similar to that found in an intense hurricane. The geometric disparity between a hurricane and the apparatus prevents strict dynamical similitude; however, the characteristic Reynolds number of the experimental flow is sufficiently large ($Re \approx 7000$) to enter a quasi-inviscid regime. With a core aspect ratio less than unity and a ratio of maximum-mean tangential to maximum-mean radial velocity (in the inflow layer) of 2.5, the experimentally generated mean flow is kinematically similar to what is known about the mean boundary layer inflow of an intense hurricane. As an additional check on the similarity of the experimental flow to a real hurricane, the radius-to-width ratio of the curvilinear shear layer in the experimental 'eye' region is in the range of values observed in real hurricanes. A study of the dependence of the forced asymmetric flow on this radius-to-width ratio is planned in forthcoming work.

Maintained by the convergence of circulation from the vortex periphery and 'downwelling' in the centre, the core flow comprises two quasi-steady vortices that coexist with a quasi-circular shear layer, intermittant secondary vortices and spiral-like filaments outside the main shear layer. In the frame of reference rotating with the primary vortices, the maximum tangential velocity of these vortices is found to be comparable to the maximum tangential velocity of the parent mean vortex. The maximum tangential velocity of the 'low-level' flow is found to be approximately 1.5 times that of the azimuthal and temporal mean tangential velocity. Given the idealizations of the experimental setup, the velocity enhancement associated with the

vortices may serve as an upper bound in practical situations. For comparison, this enhancement is less than the factor of 2 considered typical of suction vortices in intense tornadoes (Fujita 1971; Rotunno 1984; Fiedler 1998). We currently lack a theory that predicts the structure and intensity of mesovortices in both hurricanes and tornadoes.

In comparison to a real hurricane there is a potential limitation of the laboratory setup that deserves mention. While the eyewall in a real hurricane is nearly neutrally stratified (Emanuel 1986), the eye is stably stratified (Smith 1980; Willoughby 1998). In the present experiment, however, the fluid is everywhere homogeneous (neutrally stratified). The rate at which nearly stagnant air is supplied to the base of the core flow in a real hurricane may consequently tend to be impeded by stratification in the eye. In view of this difference, then, a concern is that hurricane mesovortices might tend to spin up the eye to solid body rotation more rapidly than in the experimental flow. However, the tendency of coherent mesovortices to propagate inward to the centre of circulation (thereby spinning up the eye to approximate solid body rotation) may also be suppressed due to the tendency of the mesovortices to propagate 'up' the radial vorticity gradient of the azimuthal mean flow that supports them. This effect is analogous to the tendency of an intense 'cyclonic' vortex to propagate up its ambient vorticity gradient (Reznik & Dewar 1994; Montgomery, Moller & Nicklas 1999 and references therein), but here the shearing dynamics across the mesovortices must be taken into account (Schecter & Dubin 2001). Although detailed examination of this propagation effect in real hurricanes and the experimental flow requires further study, we believe this effect should reduce the discrepancies between the experimental flow and a real hurricane. Flight-level observations suggest that during hurricane intensification the tendency to spin up the eye to solid body rotation is more than compensated by vortex-tube stretching in the eyewall; this generates an annulus of elevated vorticity in the storm's eyewall (Kossin & Eastin 2001; Kossin & Schubert 2001; cf. figure 16). The tendency of the experimental flow to maintain the strong mean vorticity near the 'eyewall' should thus be similar to a real hurricane, at least during the intensification phase.

Our findings support the hypothesis that intense hurricanes contain coherent vortex structures with significantly stronger near-surface winds locally than the parent vortex. If the findings are found to be consistent with future *in-situ* observations, it would indicate the need to recognize the potential hazard of intense mesovortices in construction codes and emergency management planning for coastal regions threatened by intense landfalling storms.

The experiment furnishes new insight into the fluid dynamics of two-celled vortex flows that possess a core aspect ratio less than unity. Despite the presence of a relatively strong secondary circulation through the primary vortex, the rotational part of the horizontal velocity field is found to be approximately two-dimensional. The high vorticity of the core flow together with an aspect ratio less than unity is evidently sufficient to 'rotationally stratify' the flow even in a local environment possessing strong differential rotation. A two-dimensional eigenvalue analysis is consistent with this interpretation, predicting for the benchmark flow a wavenumber 2 vorticity asymmetry whose structure and rotation rate are roughly consistent with that of the primary mesovortices. These instability predictions are consistent with previous work by Vladimirov & Tarasov (1980), Lugovtsov (1982), Gall (1983), and Nolan & Montgomery (2002). This work suggests that for hurricane-like vortices with secondary circulation, the multiple vortex phenomenon and attendant large-scale structures are governed by quasi-two-dimensional fluid dynamics.

This research was supported in part by NOAA Grant NA67RJ0152, Amendment 19, NSF ATM-0101781 and Colorado State University. M. M. would like to express his gratitude to Professors S. Cheng and A. Lau of the Mathematics Department, Hong Kong University of Science and Technology (HKUST), for their hospitality that enabled the completion of the experimental phase of this work. M. M. would also like to thank Dr F. Marks of NOAA/AOML's Hurricane Research Division in Miami, FL and CSU colleagues for constructive feedback on an earlier version of the manuscript; and L. K. P., M. P. M., R. P., and S. P. for their support during his visit to HKUST. The authors thank Dr K. Emanuel for making his 1995 hurricane model available to us and for making several suggestions in his review that helped improve the presentation; Mr J. Camp for generating figure 8(*b*); and Mr W. Terwey for assistance with the calculations of § 9, together with B. McNoldy, A. Kankewicz, and CSU/CIRA for providing the Hurricane Alberto image and two anonymous reviewers for their constructive comments.

REFERENCES

Adrian, R. J. 1991 Particle-imaging techniques for experimental fluid mechanics. *Annu. Rev. Fluid Mech.* **23**, 261–304.

Bassom, A. P. & Gilbert, A. D. 1999 The spiral wind-up and dissipation of vorticity and a passive scalar in a strained planar vortex. *J. Fluid Mech.* **398**, 245–270.

Batchelor, G. K. 1967 *An Introduction to Fluid Dynamics*. Cambridge University Press.

Black, P. G. & Marks, F. D. 1991 The structure of an eyewall meso-vortex in Hurricane Hugo (1989). *Conference Proc. Am. Met. Soc., Hurr. and Trop. Met., Miami, FL*, pp. 579–582.

Braun, S. A. 2002 A cloud-resolving simulation of Hurricane Bob (1991): Storm structure and eyewall buoyancy. *Mon. Wea. Rev.* **130**, 1573–1592.

Braun, S. A. & Tao, W. K. 2000 Sensitivity of high-resolution simulations of Hurricane Bob (1991) to planetary boundary layer parameterizations. *Mon. Wea. Rev.* **128**, 3941–3961.

Chen, Y. & Yau, M. K. 2001 Spiral bands in a simulated hurricane. Part I: Vortex Rossby Wave Verification. *J. Atmos. Sci.* **58**, 2128–2145.

Church, C. R., Snow, J. T. & Agee, E. M. 1977 Tornado vortex simulation at Purdue University. *Bull. Am. Met. Soc.* **58**, 900–908.

Drazin, P. G. & Reid, W. H. 1981 *Hydrodynamic Stability*. Cambridge University Press.

Eliassen, A. & Lystad, M. 1977 The Ekman layer of a circular vortex. A numerical and theoretical study. *Geophysica Norvegica* **31**, 1–16.

Emanuel, K. A. 1984 A note on the stability of columnar vortices. *J. Fluid Mech.* **145**, 235–238.

Emanuel, K. A. 1986 An air–sea interaction theory for tropical cyclones. *J. Atmos. Sci.* **43**, 1062–1071.

Emanuel, K. A. 1989 The finite amplitude nature of tropical cyclogenesis. *J. Atmos. Sci.* **46**, 3431–3456.

Emanuel, K. A. 1995 Sensitivity of tropical cyclones to surface exchange coefficients and a revised steady-state model incorporating eye dynamics. *J. Atmos. Sci.* **52**, 3969–3976.

Emanuel, K. A. 1997 Some aspects of hurricane inner-core dynamics and energetics. *J. Atmos. Sci.* **54**, 1014–1026.

Emanuel, K. A. 1998 Theoretical and numerical modeling inferences on the feedback of ocean dynamics on hurricane intensity. *Symp. on Tropical Cyclone Intensity Change, Phoenix, AZ*, Preprints, pp. 154–160. American Meteorological Society.

Fiedler, B. 1998 Wind-speed limits in numerically simulated tornadoes with suction vortices. *Q. J. R. Met. Soc.* **124**, 2377–2392.

Finley, C. 1997 Numerical simulation of intense small-scale vortices generated by supercell thunderstorms. PhD dissertation, Dept. of Atmospheric Science, Colorado State University.

Frank, W. M. 1984 A composite of the core of a mature hurricane. *Mon. Wea. Rev.* **112**, 2401–2420.

Fujita, T. T. 1971 Proposed mechanism for suction spots accompanied by tornadoes. *7th Conf. Severe Local Storms, Kansas City*, Preprints, pp. 208–213. American Meteorological Society.

Gall, R. L. 1983 A linear analysis of the multiple vortex phenomenon in simulated tornadoes. *J. Atmos. Sci.* **40**, 2010–2024.

Gall, R. L., Tuttle, J. & Hildebrand, P. 1998 Small-scale spiral bands observed in Hurricanes Andrew, Hugo, and Erin. *Mon. Wea. Rev.* **126**, 1749–1766.

Gent, P. & McWilliams, J. 1986 The instability of barotropic circular vortices. *Geophys. Astrophys. Fluid Dyn.* **35**, 209–233.

Gray, W. M. 1979 Hurricanes: Their formation, structure, and likely role in the tropical circulation. *Meteorology Over the Tropical Oceans* – Supplement (ed. D. B. Shaw), pp. 155–218. RMS: James Glaisher House, Grenville Place, Bracknell, Berkshire, RG12 1BX, UK.

Gray, W. M. & Shea, D. J. 1973 The hurricane's inner core region. Part II: Thermal stability and dynamic characteristics. *J. Atmos. Sci.* **30**, 1565–1576.

Greenspan, H. P. 1968 *The Theory of Rotating Fluids*. Cambridge University Press.

Guinn, T. A. & Schubert, W. H. 1993 Hurricane spiral bands. *J. Atmos. Sci.* **50**, 3380–3403.

Hasler, A. F., Black, P. G., Karyampudi, V. M., Jentoft-Nielson, M., Palaniappenan, K. & Chesters, D. 1997 Synthesis of eyewall mesovortex and supercell convective structures in Hurricane Luis with GOES-8/9 stereo, concurrent 1-min GOES-9 and NOAA airborne radar observations. *22nd Conf. on Hurricanes and Tropical Meteorology, Ft. Collins, CO*, Preprints, pp. 201–202. American Meteorological Society.

Hausman, S. A. 2001 Formulation and sensitivity analysis of a nonhydrostatic, axisymmetric tropical cyclone model. PhD dissertation, Colorado State University, Department of Atmospheric Science.

Held, I. M. & Hou, A. Y. 1980 Nonlinear axially symmetric circulations in a nearly inviscid atmosphere. *J. Atmos. Sci.* **37**, 515–533.

Houze, R. Jr. 1993 *Cloud Dynamics*. Academic.

Howard, L. N. & Gupta, A. S. 1962 On the hydrodynamic and hydromagnetic stability of swirling flows. *J. Fluid Mech.* **14**, 463–476.

Huang, X. P., Fine, K. S. & Driscoll, C. F. 1995 Coherent vorticity holes from 2D turbulence decaying in a background shear flow. *Phys. Rev. Lett.* **74**, 4424.

Hughes, L. A. 1952 On the low-level wind structure of tropical storms. *J. Met.* **9**, 422–428.

Jin, D. Z. & Dubin, D. H. E. 1998 Regional maximum entropy theory of vortex crystal formation. *Phys. Rev. Lett.* **80**, 4434–4437.

Kossin, J. P., McNoldy, B. D. & Schubert, W. H. 2002 Vortical swirls in hurricane eye clouds. *Mon. Wea. Rev.*, In press.

Kossin, J. P. & Eastin, M. E. 2001 Two distinct regimes in the kinematic and thermodynamic structure of the hurricane eye and eyewall. *J. Atmos. Sci.* **58**, 1079–1090.

Kossin, J. P. & Schubert, W. H. 2001 Mesovortices, polygonal flow patterns, and rapid pressure falls in hurricane-like vortices. *J. Atmos. Sci.* **58**, 2196–2209.

Kossin, J. P., Schubert, W. H. & Montgomery, M. T. 2000 Unstable interactions between a hurricane's primary eyewall and a secondary ring of enhanced vorticity. *J. Atmos. Sci.* **57**, 3893–3917.

Kuo, H. L. 1959 Dynamics of convective vortices and eye formation. *The Atmosphere and Sea in Motion* (ed. B. Bolin), pp. 413–424. Rockefeller Institute Press.

Leibovich, S. & Stewartson, K. 1983 A sufficient condition for the instability of columnar vortices. *J. Fluid Mech.* **126**, 335–356.

Lindzen, R. S. 1992 *Dynamics in Atmospheric Physics*. Cambridge University Press.

Lugovtsov, B. A. 1982 Laboratory models of tornado-like vortices. In *Intense Atmospheric Vortices* (ed. X. X. Bengtsson & M. J. Lighthill). Springer.

Malkus, J. S. 1958 On the structure of the mature hurricane eye. *J. Met.* **15**, 337–349.

Malkus, J. S. & Riehl, H. 1960 On the dynamics and energy transformations in steady-state hurricanes. *Tellus*, **12**, 1–20.

Marks, F. D. & Black, P. G. 1990 Close encounter with an intense mesoscale vortex within Hurricane Hugo (September 15, 1989). *Fourth Conf. on Mesoscale Processes, Boulder, CO, June 25-20 1990*, pp. 114–115. American Meteorological Society.

McWilliams, J. C. 1985 A uniformly valid model spanning the regimes of geostrophic and isotropic, stratified turbulence: Balanced turbulence. *J. Atmos. Sci.* **42**, 1773–1774.

Melander, M. V., McWilliams, J. C. & Zabusky, N. J. 1987 Axisymmetrization and vorticity gradient intensification of an isolated two-dimensional vortex. *J. Fluid Mech.* **178**, 137–159.

Michalke, A. & Timme, A. 1967 On the inviscid instability of certain two-dimensional vortex-type flows. *J. Fluid Mech.* **29**, 647–666.

Möller, J. D. & Montgomery, M. T. 2000 Tropical cyclone evolution via potential vorticity anomalies in a three-dimensional balance model. *J. Atmos. Sci.* **57**, 3366–3387.

Montgomery, M. T. & Kallenbach, R. J. 1997 A theory for vortex Rossby waves and its application to spiral bands and intensity changes in hurricanes. *Q. J. R. Met. Soc.* **123**, 435–465.

Montgomery, M. T., Moller, J. D. & Nicklas, C. T. 1999 Linear and nonlinear vortex motion in an asymmetric balance shallow water model. *J. Atmos. Sci.* **56**, 749–768.

Morton, B. R. 1966 Geophysical vortices. *Prog. Aeronaut. Sci.* **7**, 145–194.

Nolan, D. & Montgomery, M. T. 2002 Nonhydrostatic, three-dimensional perturbations to balanced, hurricane-like vortices. Part I: Linearized formulation, stability, and evolution. *J. Atmos. Sci.* **59**, In press.

Ooyama, K. V. 1969 Numerical simulation of the life cycle of tropical cyclones. *J. Atmos. Sci.* **26**, 3–40.

Ooyama, K. V. 1982 Conceptual evolution of the theory and modeling of the tropical cyclone. *J. Met. Soc. Japan* **60**, 369–379.

Pearce, R. P. 1992 A critical review of progress in tropical cyclone physics including experimentation with numerical models. In *ICSU/WMO Intl Symp. on Tropical Cyclone Disasters*, pp. 45–60. Peking University Press.

Powell, M. D. 1982 The transition of the Hurricane Frederic boundary layer wind field from the open Gulf of Mexico to landfall. *Mon. Wea. Rev.* **110**, 1912–1932.

Powell, M. D. & Houston, S. H. 1996 Hurricane Andrew's landfall in South Florida. Part II: Surface wind fields and potential real-time applications. *Weather and Forecasting* **11**, 329–349.

Rayleigh, Lord 1916 The dynamics of revolving flows. *Proc. R. Soc. Lond.* A **93**, 148–154.

Reasor, P. D., Montgomery, M. T., Marks, F. D. Jr. & Gamache, J. F. 2000 Low-wavenumber structure and evolution of the hurricane inner core observed by airborne dual-doppler radar. *Mon. Wea. Rev.* **128**, 1653–1680.

Reznik, G. M. & Dewar, W. K. 1994 An analytical theory of distributed axisymmetric barotropic vortices on the beta plane. *J. Fluid Mech.* **269**, 301–321.

Riehl, H. 1954 *Tropical Meteorology*. McGraw-Hill.

Riehl, H. 1963 Some relations between wind and thermal structure of steady state hurricanes. *J. Atmos. Sci.* **20**, 276–287.

Rotunno, R. 1978 A note on the stability of a cylindrical vortex sheet. *J. Fluid Mech.* **87**, 761–771.

Rotunno, R. 1984 An investigation of a three-dimensional asymmetric vortex. *J. Atmos. Sci.* **41**, 283–298.

Rotunno, R. & Emanuel, K. A. 1987 An air–sea interaction theory for tropical cyclones. Part II: Evolutionary study using a nonhydrostatic axisymmetric numerical model. *J. Atmos. Sci.* **44**, 542–560.

Schecter, D. A. & Dubin, D. H. E. 2001 Theory and simulations of vortex motion driven by a background vorticity gradient. *Phys. Fluids* **13**, 1704–1723.

Schecter, D. A., Dubin, H. E., Cass, A. C., Driscoll, C. F., Lansky, I. M. & O'Neil, T. M. 2000 Inviscid damping of asymmetries on a two-dimensional vortex. *Phys. Fluids* **12**, 2397–2412.

Schecter, D. A., Dubin, D. H. E., Fine, K. S. & Driscoll, C. F. 1999 Vortex crystals from 2D flow: Experiment and simulation. *Phys. Fluids* **11**, 905–914.

Schlichting, H. 1960 *Boundary Layer Theory*. McGraw Hill.

Schneider, E. 1977 Axially symmetric steady state models of the basic state of instability and climate studies. Part II: Nonlinear calculations. *J. Atmos. Sci.* **34**, 280–296.

Schubert, W. H., Montgomery, M. T., Taft, R. K., Guinn, T. A., Fulton, S. R., Kossin, J. P. & Edwards, J. P. 1999 Polygonal eyewalls, asymmetric eye contraction, and potential vorticity mixing in hurricanes. *J. Atmos. Sci.* **56**, 1197–1223.

Shapiro, L. J. 1983 The asymmetric boundary layer flow under a translating hurricane. *J. Atmos. Sci.* **40**, 1984–1998.

Shapiro, L. J. 2000 Potential vorticity asymmetries and tropical cyclone evolution in a moist three-layer model. *J. Atmos. Sci.* **57**, 3645–3662.

Shapiro, L. J. & Montgomery, M. T. 1993 A three-dimensional balance theory for rapidly rotating vortices. *J. Atmos. Sci.* **50**, 3322–3335.

Shapiro, L. J. & Willoughby, H. E. 1982 The response of balanced hurricanes to local sources of heat and momentum. *J. Atmos. Sci.* **39**, 378–394.

Sinclair, P. C. 1973 The lower structure of dust devils. *J. Atmos. Sci.* **30**, 1599–1619.

Smith, R. K. 1980 Tropical cyclone eye dynamics. *J. Atmos. Sci.* **37**, 1227–1232.

Stewart, S. R. & Lyons, S. W. 1996 A WSR-88D radar view of tropical cyclone Ed. *Weather and Forecasting* **11**, 115–135.

Stewart, S. R., Simpson, J. & Wolff, D. 1997 Convectively-induced mesocyclonic vortices in the eyewall of tropical cyclones as seen by WSR-88D Doppler radars. *22nd Conf. on Hurricanes and Tropical Meteorology, Ft. Collins, CO*, Preprints, pp. 106–108. American Meteorological Society.

Vladimirov, V. A. & Tarasov, V. F. 1980 Formation of a system of vortex filaments in a rotating liquid. *Izv. Akad. Az. Nauk SSSR, Mekh. Zhid. i Gaza* **1**, 44–51 (referred to herein as VT).

Wakimoto, R. M. & Black, P. G. 1994 Damage survey of Hurricane Andrew and its relationship to the eyewall. *Bull. Am. Met. Soc.* **75**, 189–200.

Wan, C. A. & Chang, C. C. 1972 Measurement of the velocity field in a simulated tornado-like vortex using a three-dimensional velocity probe. *J. Atmos. Sci.* **29**, 116–127.

Wang, Y. 2002*a* Vortex Rossby waves in a numerically simulated tropical cyclone. Part I: Overall structure, potential vorticity, and kinetic energy budgets. *J. Atmos. Sci.* **59**, 1213–1238.

Wang, Y. 2002*b* Vortex Rossby waves in a numerically simulated tropical cyclone. Part II: The role in tropical cyclone structure and intensity changes. *J. Atmos. Sci.* **59**, 1239–1262.

Ward, N. B. 1972 The exploration of certain features of tornado dynamics using a laboratory model. *J. Atmos. Sci.* **29**, 1194–1204.

Weske, J. R. & Rankin, T. M. 1963 Generation of secondary motions in the field of a vortex. *Phys. Fluids* **6**, 1397–1403.

Whitehead, J. A. Jr & Porter, D. L. 1978 Axisymmetric critical withdrawal of a rotating fluid. *Dyn. Atmos. Oceans* **2**, 1–18.

Willoughby, H. E. 1998 Tropical cyclone eye thermodynamics. *Mon. Wea. Rev.* **126**, 1653–1680.

Willoughby, H. E. 1990 Gradient balance in tropical cyclones. *J. Atmos. Sci.* **47**, 265–274.

Willoughby, H. E. 1979 Forced secondary circulations in hurricanes. *J. Geophys. Res.* **84**, 3173–3183.

Willoughby, H. E. & Black, P. G. 1996 Hurricane Andrew in Florida: Dynamics of a disaster. *Bull. Am. Met. Soc.* **77**, 543–549.

Wurman, J. & Winslow, J. 1998 Intense sub-kilometer-scale boundary layer rolls observed in Hurricane Fran. *Science* **280**, 555–557.